J. Fluid Mech. (1988), *vol.* 187, *pp.* 533–571
Printed in Great Britain

The dynamics of towed flexible cylinders Part 2. Negatively buoyant elements

By A. P. DOWLING

Department of Engineering, University of Cambridge, Trumpington Street, Cambridge CB2 1PZ, UK

(Received 20 March 1987)

A ship, towing a heavier-than-water cable with a neutrally buoyant slender cylinder attached to the downstream end of the cable, is considered. The neutrally buoyant element contains a sonar array. Linear changes in the ship's velocity cause perturbations of both the cable and cylinder. The form of transverse vibrations of the neutrally buoyant cylinder was determined in Part 1. The propagation of disturbances along the cable is investigated in this paper. In particular, the effectiveness of the cable at isolating the sonar array from forcing due to unsteady ship motion is examined.

The cable and cylinder are found to be stable under constant towing conditions. It is therefore appropriate to investigate their response to forcing. Meanderings in the ship's track produce transverse displacements of both the cable and the cylinder. These transverse oscillations entirely decouple from any in-plane motion. The propagation of disturbances of frequency ω along the cable depends strongly on the value of the non-dimensional frequency $\omega l_C/U$, where l_C is the cable length and U is the towing speed, and only weakly on the other cable parameters. The cable acts as an effective low-pass filter to transverse oscillations, the amplitude of disturbances with non-dimensional frequency greater than 10 being reduced by at least 90% as they propagate along the cable.

Unsteadiness in the ship's speed can result in in-plane deflections of the cable, and vertical oscillations of the cylinder containing the sonar array. In contrast to the transverse oscillations a significant proportion of the in-plane disturbances at the ship travels to the sonar array at all values of the frequency. Low- and high-frequency analytical forms are derived to explain why this occurs. Perturbations in the ship's position are most effectively transformed into vertical oscillations of the array at a frequency of $2.8U/l_C$. The effect of cable properties on transmission along the cable is investigated. The transmission again depends on the value of the non-dimensional frequency $\omega l_C/U$. Parameter changes, which increase the cable critical angle, increase the proportion of the disturbance at the towing point that is transformed into vertical array motion, for a fixed value of $\omega l_C/U$. This is explained by reference to the low- and high-frequency analytical solutions.

1. Introduction

The dynamics of an instrumentation package being towed by a ship are investigated. The towed system consists of a long, slender neutrally buoyant cylinder, containing a sonar array, attached to a ship by a heavy tow-cable. When the ship maintains a constant velocity the sonar array is straight and horizontal. However changes in the ship's velocity make both the cable and the array deform.

We analyse linear departures from the steady towing case. Dowling (1988, hereinafter referred to as Part 1) determines the form of linear displacements of the neutrally buoyant cylinder. The propagation of disturbances along the cable is investigated in this paper. One aim of the work is to provide a simple means by which the shape of the towed system can be predicted from the ship's path. An ideal cable would attenuate disturbances, in order to isolate the sonar array from the effects of unsteady ship motion. The way in which the cable parameters should be chosen to enhance this attenuation is investigated.

The cable, being heavier than water, is inclined at an angle to the towing direction over most of its length. Its downstream end, however, must be horizontal in the mean, as it is attached to a neutrally buoyant cylinder. Païdoussis (1966, 1968, 1973) derived an equation for the linearized transverse displacement of a towed neutrally buoyant element. Kennedy & Strahan (1981) modified Païdoussis' equation in an *ad hoc* way to describe the propagation of horizontal transverse displacements along a heavy cable. They just changed the drag coefficients in Païdoussis' equation to values more appropriate for a cable at an appreciable angle to the flow. This does not, of course, account for all the effects of cable inclination. But Kennedy & Strahan were able to obtain some agreement between such calculations and their experimental results. This approach is not suitable for in-plane oscillations where, for a curved cable, displacements normal and tangential to the mean cable position couple to unsteady tensions.

In a series of papers Huffman & Genin (1971) and Cannon & Genin (1972*a*, *b*) derive equations to describe linear perturbations of a cable in a related problem, a tow-cable attached to a heavy mass in air. Their choice of variables makes the problem seem rather complicated, since they have four variables describing transverse cable motion and five for its in-plane motion. The stability of the towed body is investigated and they find it to be always stable. Schram & Reyle (1968) determine the dynamic response of a cable towing a heavy body to nonlinear disturbances of the towing point. They use the method of characteristics to obtain a numerical solution.

We adopt a different approach. The cable motion is described in terms of displacements normal and tangential to the mean cable position and the unsteady tension. Equations of motion for linear perturbations of the cable from its configuration in steady towing are derived in §2. These are a natural extension of Païdoussis' work, and his equation can be recovered as the specific gravity of the cable approaches unity. Transverse oscillations decouple from any in-plane vibration. For disturbances with time dependence $e^{i\omega t}$ the equations may be integrated in a straightforward way to determine the spatial development of cable displacement. The form for the deflections of the neutrally buoyant cylinder calculated in Part 1 specifies the downstream boundary condition for the cable motion.

The tension in the cable is sufficiently large to ensure that over most of its length the mean cable geometry is a straight line, inclined at the critical angle to the horizontal. This is the angle of inclination for which the mean normal drag and gravity forces on the cable balance. Phillips (1949) considered the stability of a cable with uniform tension inclined at an angle to an oncoming flow. Zajac (1957) investigated the propagation of disturbances down such a cable and Lyon (1962) went on to include a linear variation in tension. Our equations for both transverse and in-plane motion reduce to Lyon's when the cable angle is constant and a term due to cable weight is neglected. Over the range where the cable inclination is fixed, the differential equations for cable motion are sufficiently simple to enable analytical

forms to be derived in the limit of low and high frequency. These asymptotic solutions are useful when interpreting effects observed in the numerical solutions.

Transverse cable oscillations are considered in §3, the in-plane motions being determined in §4. The stability of the cable and neutrally buoyant cylinder under steady towing is investigated by seeing whether free modes, in which there is no perturbation in the position of the upstream end of the cable, grow or decay in time. If all the eigenfrequencies have positive imaginary parts, any disturbance decays with time and the system is stable. Any eigenfrequency with negative imaginary part, however, represents a growing mode making the towed cable and cylinder unstable. It is demonstrated that there are no eigenfrequencies in the lower half Ω-plane and hence the acoustic streamer is stable to towing. It is therefore appropriate to investigate its response to forcing. A ship following a meandering track causes a transverse motion of the upstream end of the cable. The deflections this produces in the rest of the cable are determined in §3. It is found that at low frequencies these disturbances propagate down the cable with little attenuation, while at higher frequencies they decay. The details of the form of the cable motion are of limited interest. What is relevant is how much vibration is transferred from the ship to the sonar array along the cable. We investigate this by calculating the ratio of the disturbance at the downstream end of the cable to that at its upstream end, at a particular frequency ω. This transfer function is found to depend strongly on the value of the non-dimensional frequency $\omega l_{\mathrm{C}}/U$, where l_{C} is the cable length and U the towing speed, and only weakly on the other cable parameters. The magnitude of the transfer function decreases as $\omega l_{\mathrm{C}}/U$ is increased. Disturbances with a non-dimensional frequency greater than 10 are reduced in amplitude by at least 90% as they propagate along the cable. Kennedy & Strahan (1981) measured this transfer function in experiments at sea. Our calculated form is in very good agreement with their data.

In-plane oscillations of the cable and cylinder are investigated in §4. These can be excited by unsteadiness in ship speed which produces a horizontal displacement in the position of the upstream cable end. The disturbances propagate down the cable and cause both horizontal and vertical displacements of the sonar array. A significant proportion of the disturbance at the ship is found to travel to the array at all frequencies. The low- and high-frequency analytic solutions are used to explain why this occurs. Perturbations in the ship's position are most effectively transformed into vertical oscillations of the array at a frequency of $2.8U/l_{\mathrm{C}}$. The effect of cable properties on transmission along the cable is investigated. Parameter changes, which increase the cable critical angle, increase the proportion of the disturbance to the towing point that is transformed into vertical array motion, for a fixed value of $\omega l_{\mathrm{C}}/U$. This is explained by reference to the low- and high-frequency analytical solutions.

2. The equations of cable motion

Consider a cable of radius a_{C}, length l_{C}, towed in the negative x-direction through still fluid at a speed U with a neutrally buoyant cylinder attached to its downstream end. The z-axis is chosen to be vertically downwards. The y-axis is therefore horizontal and perpendicular to the direction of motion. Since the cable is heavier than the surrounding water, it is inclined at an angle to the direction of motion over most of its length. Let l denote arc length along the cable, $\boldsymbol{r}(l, t)$ the position vector

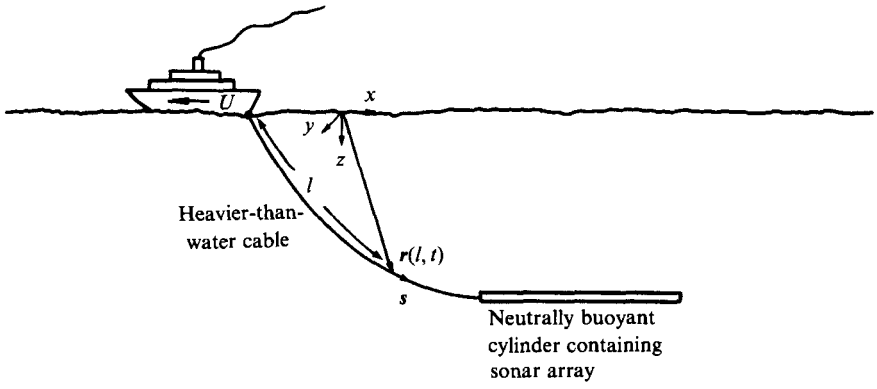

FIGURE 1. Typical geometry for a ship towing an array.

of the cable element l at time t, and $\boldsymbol{s}$ the tangential unit vector, $\boldsymbol{s} = \partial \boldsymbol{r}/\partial l$, as shown in figure 1. Then the equation of motion of the cable is

$$\rho_0 \sigma \pi a_C^2 \boldsymbol{A} = \rho_0 \sigma \pi a_C^2 \boldsymbol{g} + \frac{\partial}{\partial l}(T\boldsymbol{s}) + \boldsymbol{F}, \tag{2.1}$$

$\boldsymbol{A} = \ddot{\boldsymbol{r}}$ is the acceleration of the cable element, where the dot denotes a time derivative. σ is the specific gravity of the cable and ρ_0 the density of water. $\rho_0 \sigma \pi a_C^2$ is therefore the mass per unit length of cable. $\boldsymbol{g}$ is the acceleration due to gravity. $T(l)$, the tension in the cable, changes along its length. The force exerted on unit length of cable by the surrounding fluid is denoted by $\boldsymbol{F}$. This force $\boldsymbol{F}$ is made up of a buoyancy term $-\rho_0 \pi a_C^2 \boldsymbol{g}$, a virtual mass term equal and opposite to the force required to accelerate the fluid, and drag which opposes the velocity of the cable. We take the virtual mass term to be $-\rho_0 \pi a_C^2 \boldsymbol{A}_n$ where $\boldsymbol{A}_n$ is the normal cable acceleration, $\boldsymbol{A}_n = \boldsymbol{A} - (\boldsymbol{A} \cdot \boldsymbol{s})\boldsymbol{s}$. The drag can be conveniently decomposed into its components tangential and normal to the local cable axis. We are interested in cable oscillations with frequencies very much lower than the typical vortex shedding frequency from the cable. It is therefore appropriate to use a quasi-static form for the drag. As in Part 1 and following Taylor (1952) we introduce

$$D_T = \tfrac{1}{2}\rho_0 |\boldsymbol{v}|^2 2\pi a_C C_T \cos i, \tag{2.2a}$$

and

$$D_N = \tfrac{1}{2}\rho_0 |\boldsymbol{v}|^2 (2a_C C_D \sin^2 i + 2\pi a_C C_N \sin i), \tag{2.2b}$$

as the tangential and normal components of the drag per unit cable length. $\boldsymbol{v}$, the velocity of the cable element, is equal to $\dot{\boldsymbol{r}}$, and i, the angle of incidence of the cable is defined by

$$|\boldsymbol{v}| \cos i = \boldsymbol{v} \cdot \boldsymbol{s}, \quad |\boldsymbol{v}| \sin i = |\boldsymbol{v} \times \boldsymbol{s}|. \tag{2.3}$$

The tangential drag leads to tension in the cable and as discussed in Part 1 the value of the tangential drag coefficient can be deduced from measurements of this tension. Data suggest $C_T = 0.0025$ to be reasonable. Both form drag and skin-frictional forces contribute to the normal drag. The Engineering Sciences Data Item No. 80025 gives $C_D = 1.2$ for flow past an inclined cylinder at effective Reynolds numbers less than 3×10^5. There is less evidence to determine an appropriate value for the drag coefficient C_N, and as in Part 1 the effect of varying C_N in the range $0 \leqslant C_N \leqslant C_T$ will be investigated.

Substitution for the fluid forces from (2.2) and (2.3) into (2.1) leads to the general equation of motion of the cable. Since the fluid forces naturally decompose into their components tangential and normal to the cable axis, we will introduce the notation v_s and $\boldsymbol{v}_n$ to denote the components of $\boldsymbol{v}$ tangential and normal to $\boldsymbol{s}$ respectively, i.e. $v_s = \boldsymbol{v}\cdot\boldsymbol{s}$ and $\boldsymbol{v}_n = \boldsymbol{v} - v_s\boldsymbol{s}$. Components $g_s = \boldsymbol{g}\cdot\boldsymbol{s}$ and $\boldsymbol{g}_n = \boldsymbol{g} - g_s\boldsymbol{s}$ are defined in a similar way. Then the equation of motion for the cable can be rewritten as

$$\rho_0 \sigma \pi a_C^2 \boldsymbol{A}_s = \rho_0(\sigma-1)\pi a_C^2 g_s + \frac{\partial T}{\partial l} - \rho_0 |\boldsymbol{v}| \pi a_C C_T v_s, \tag{2.4a}$$

and

$$\rho_0(\sigma+1)\pi a_C^2 \boldsymbol{A}_n = \rho_0(\sigma-1)\pi a_C^2 \boldsymbol{g}_n + T\frac{\partial \boldsymbol{s}}{\partial l} - \rho_0 a_C(C_D|\boldsymbol{v}_n| + \pi C_N|\boldsymbol{v}|)\boldsymbol{v}_n. \tag{2.4b}$$

This equation is to be solved subject to boundary conditions at $l = 0$ and l_C. The downstream end of the cable is attached to a neutrally buoyant cylinder containing the sonar array. Their displacements must be equal at the junction, i.e. $\boldsymbol{r}(l_C, t)$ is continuous across the join of the cable and the cylinder

$$[\boldsymbol{r}(l_C, t)]^{\text{cable}}_{\text{cylinder}} = \boldsymbol{0}. \tag{2.5}$$

If the join is so short that it has negligible inertia, the forces acting on it must balance. The fluid dynamical forces acting on the junction between two cylinders of different radii were discussed in Part 1. The largest fluid force is that due to the virtual mass of the cylinder, but even this is small in comparison with the tension forces. These are appreciable at the upstream end of the towed cylinder because they balance the longitudinal drag on the whole cylinder. The condition that the forces on the junction of the cable and the cylinder must be in equilibrium therefore reduces to a statement that

$$[T\boldsymbol{s}]^{\text{cable}}_{\text{cylinder}} = \boldsymbol{0}. \tag{2.6}$$

Since $|\boldsymbol{s}| = 1$, this vector equation implies that T is to be continuous and so is the slope of the cylinders' centreline.

Equations (2.4)–(2.6) will first be used to determine the mean position of the cable. For a constant towing speed U in the negative x-direction, it is appropriate to seek a solution in which the cable parameters are constant, $\boldsymbol{v} = (-U, 0, 0)$, $T = \bar{T}(l)$ and $\boldsymbol{s} = \bar{\boldsymbol{s}} = (\cos\bar{\theta}, 0, \sin\bar{\theta})$ say. Then since there is no acceleration, equation (2.4*a*) reduces to a condition that the tension, gravity and fluid dynamical forces balance:

$$\frac{\partial \bar{T}}{\partial l} = -\rho_0(\sigma-1)\pi a_C^2 g \sin\bar{\theta} - \rho_0 U^2 \pi a_C C_T \cos\bar{\theta}. \tag{2.7}$$

The normal equation (2.4*b*) only has one non-zero component. It is in the direction $(-\sin\bar{\theta}, 0, \cos\bar{\theta})$ and gives

$$\bar{T}\frac{\mathrm{d}\bar{\theta}}{\mathrm{d}l} = -\rho_0(\sigma-1)\pi a_C^2 g \cos\bar{\theta} + \rho_0 a_C U^2(C_D \sin\bar{\theta} + \pi C_N)\sin\bar{\theta}. \tag{2.8}$$

At its downstream end the cable is joined to a cylinder which is neutrally buoyant. The mean position of that cylinder is horizontal and parallel to the x-axis. The tension at the leading edge of a neutrally buoyant cylinder of radius a_A, length l_A with a free downstream end was given by Part 1, equation (2.6) as $\rho_0 \pi U^2 C_T a_A l_A$. The

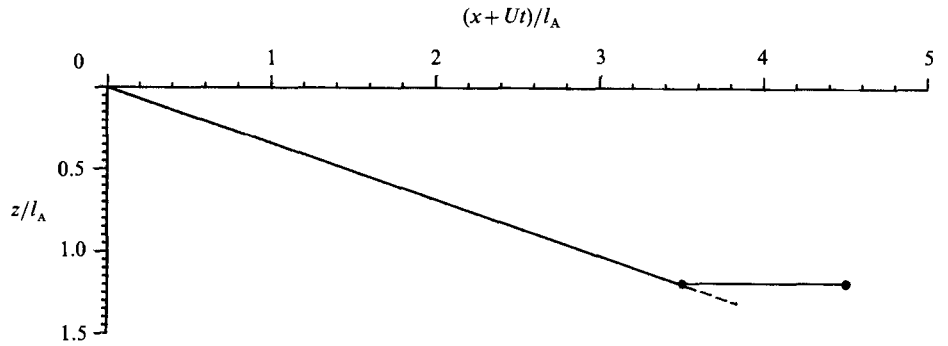

FIGURE 2. The mean configuration of the cable and neutrally buoyant cylinder under constant towing for $C_T = 0.0025$, $C_D = 1.2$, $C_N = 0.75C_T$, $\sigma = 2.8$, $l_C/l_A = 3.7$, $gl_A/U^2 = 578$, $a_C/l_A = 4.125 \times 10^{-5}$ and $a_A/l_A = 8.25 \times 10^{-5}$. •, ends of the cylinder; ---, straight line at the critical angle $\bar{\theta}_c$ (defined in equation (2.11)).

mean values of the boundary conditions described by (2.5) and (2.6) are therefore simply

$$\bar{T}(l_C) = \rho_0 \pi U^2 C_T a_A l_A, \tag{2.9}$$

and

$$\bar{\theta}(l_C) = 0. \tag{2.10}$$

Integration of the differential equations (2.7) and (2.8) from $l = l_C$, where $\bar{\theta}$ and $\bar{T}$ are given by (2.9) and (2.10), to $l = 0$ determines the mean position of the cable. A typical mean configuration of the cable and neutrally buoyant cylinder is shown in figure 2 for $\sigma = 2.8$, $C_T = 0.0025$, $C_D = 1.2$, $C_N = 0.75C_T$, $l_C/l_A = 3.7$, $a_C/l_A = 4.125 \times 10^{-5}$ and $gl_A/U^2 = 578$. The parameters of the cylinder are as in Part 1; $a_A/l_A C_T = 0.033$.

Equation (2.8) leads to solutions in which $\bar{\theta}$ increases rapidly near l_C. Away from the junction with the cylinder, the cable soon attains its critical angle at which the normal forces on it balance. Then $\bar{\theta}$ remains constant at an angle $\bar{\theta}_c$ say. Using the condition $d\bar{\theta}/dl = 0$ in (2.8) shows that the critical angle $\bar{\theta}_c$ is given by

$$(\sigma - 1)\frac{a_C g}{U^2}\cos\bar{\theta}_c = \left(C_N + \frac{C_D}{\pi}\sin\bar{\theta}_c\right)\sin\bar{\theta}_c. \tag{2.11}$$

The straight line $\bar{\theta} = \bar{\theta}_c$ is plotted in figure 2 for comparison with the exact solution for $\bar{\theta}(l)$. It is in excellent agreement with the solution except near the downstream end of the cable.

Now that the mean geometry of the cable and the mean forces on it during steady towing have been determined the form of linear perturbations from this configuration can be investigated. The position vector $\boldsymbol{r}(l, t)$ may be split up into its steady state value and a perturbation by writing

$$\boldsymbol{r}(l, t) = \bar{\boldsymbol{r}}(l, t) + \boldsymbol{r}'(l, t). \tag{2.12}$$

It is convenient to express $\boldsymbol{r}'$ in terms of ξ, η and ζ, perturbations in position along and perpendicular to the mean tangent to the cable;

$$\boldsymbol{r}'(l, t) = (\xi\cos\bar{\theta} - \eta\sin\bar{\theta}, \zeta, \xi\sin\bar{\theta} + \eta\cos\bar{\theta}). \tag{2.13}$$

ξ, η and ζ are all small quantities and their products may be neglected.

The instantaneous tangential direction, $\boldsymbol{s}$, can be obtained from the derivative

$\partial \boldsymbol{r}/\partial l$. The use of the condition that $\boldsymbol{s}$ is a unit vector leads to one relationship between ξ and η;

$$\frac{\partial \xi}{\partial l} = \eta \frac{\mathrm{d}\bar{\theta}}{\mathrm{d}l}. \tag{2.14}$$

The details of the derivation of this equation are given in the Appendix.

The velocity and acceleration of the cable element at (l, t) may be expressed in terms of η, ξ and ζ by differentiating (2.13). When these are substituted in the momentum equation (2.4), they lead to three equations for the cable perturbations:

$$\rho_0(\sigma+1)\pi a_{\mathrm{C}}^2 \ddot{\zeta} = -\rho_0(\sigma-1)\pi a_{\mathrm{C}}^2 g \sin\bar{\theta}\frac{\partial \zeta}{\partial l} + \bar{T}\frac{\partial^2 \zeta}{\partial l^2} - \rho_0 a_{\mathrm{C}} U(C_{\mathrm{D}}\sin\bar{\theta} + \pi C_{\mathrm{N}})\left(\dot{\zeta} + U\cos\bar{\theta}\frac{\partial \zeta}{\partial l}\right), \tag{2.15}$$

$$\rho_0 \sigma \pi a_{\mathrm{C}}^2 \ddot{\xi} = \rho_0(\sigma-1)\pi a_{\mathrm{C}}^2 g\cos\bar{\theta}\left(\frac{\partial \eta}{\partial l} + \xi\frac{\mathrm{d}\bar{\theta}}{\mathrm{d}l}\right) + \frac{\partial T'}{\partial l} - \rho_0 \pi a_{\mathrm{C}} U C_{\mathrm{T}}\left\{U\sin\bar{\theta}\left(\frac{\partial \eta}{\partial l} + \xi\frac{\mathrm{d}\bar{\theta}}{\mathrm{d}l}\right) + (1+\cos^2\bar{\theta})\dot{\xi} - \sin\bar{\theta}\cos\bar{\theta}\dot{\eta}\right\}, \tag{2.16}$$

and

$$\rho_0(\sigma+1)\pi a_{\mathrm{C}}^2 \ddot{\eta} = -\rho_0(\sigma-1)\pi a_{\mathrm{C}}^2 g\sin\bar{\theta}\left(\frac{\partial \eta}{\partial l} - \xi\frac{\mathrm{d}\bar{\theta}}{\mathrm{d}l}\right) + T'\frac{\mathrm{d}\bar{\theta}}{\mathrm{d}l} + \bar{T}\left\{\frac{\partial^2 \eta}{\partial l^2} + \eta\left(\frac{\mathrm{d}\bar{\theta}}{\mathrm{d}l}\right)^2\right\} + \rho_0 \pi a_{\mathrm{C}} U^2 C_{\mathrm{T}}\cos\bar{\theta}\frac{\mathrm{d}\bar{\theta}}{\mathrm{d}l}\xi - 2\rho_0 a_{\mathrm{C}} U C_{\mathrm{D}}\sin\bar{\theta}\left(\dot{h} + U\cos\bar{\theta}\frac{\partial \eta}{\partial l}\right) - \rho_0 \pi a_{\mathrm{C}} U C_{\mathrm{N}}\left\{(1+\sin^2\bar{\theta})\dot{\eta} - \sin\bar{\theta}\cos\bar{\theta}\dot{\xi} + U\cos\bar{\theta}\frac{\partial \eta}{\partial l}\right\}. \tag{2.17}$$

These three equations are derived in the Appendix. Together with (2.14) and appropriate boundary conditions, they specify the unsteady response of the cable. We see from (2.15) that the transverse motion completely decouples from the in-plane motion, and from (2.14), (2.16) and (2.17) that the tangential and normal in-plane deflections are related to changes in tension.

As a check, we note that if the cable were neutrally buoyant ($\sigma = 1$), its mean position would be straight and horizontal ($\bar{\theta} = 0$). Then (2.15) and (2.17) simplify considerably and Païdoussis' equation may be recovered from them.

The structure of these equations may be highlighted by writing them in non-dimensional form. We will non-dimensionalize lengths on the length of the neutrally buoyant cylinder containing the sonar array, l_{A}, and write $L = l/l_{\mathrm{A}}$. With the introduction of a non-dimensional tension $\bar{\tau} = \bar{T}/\rho_0 \pi U^2 l_{\mathrm{A}}^2$, the mean equations (2.7) and (2.8) reduce to

$$\frac{\mathrm{d}\bar{\tau}}{\mathrm{d}L} = -(\sigma-1)\epsilon^2\alpha\sin\bar{\theta} - \epsilon C_{\mathrm{T}}\cos\bar{\theta}, \tag{2.18}$$

and

$$\bar{\tau}\frac{\mathrm{d}\bar{\theta}}{\mathrm{d}L} = -(\sigma-1)\epsilon^2\alpha\cos\bar{\theta} + (\sin\bar{\theta}C_{\mathrm{D}}/\pi + C_{\mathrm{N}})\epsilon\sin\bar{\theta}. \tag{2.19}$$

$\alpha = gl_{\mathrm{A}}/U^2$ is the inverse-square of a Froude number describing the effect of gravity and $\epsilon = a_{\mathrm{C}}/l_{\mathrm{A}}$ is the small ratio of cable radius to cylinder length.

The small-amplitude perturbations satisfy the linear equations (2.14)–(2.17). For

these linear equations it is sufficient to consider each frequency separately, and we write $\zeta(l,t) = \mathrm{Re}\,(l_A \hat{\zeta}(L)\,\mathrm{e}^{\mathrm{i}\omega t})$. The non-dimensional complex amplitudes, $\hat{\xi}(L)$ and $\hat{\eta}(L)$, of the displacements $\xi(l,t)$ and $\eta(l,t)$ are defined in a similar way. The unsteady tension is written as $T'(l,t) = \mathrm{Re}\,(\rho_0 \pi U^2 l_A^2 \hat{\tau}(L)\,\mathrm{e}^{\mathrm{i}\omega t})$. It is appropriate to introduce a non-dimensional frequency $\Omega = \omega l_A/U$. Then the transverse momentum equation (2.15) describing horizontal fluctuations normal to the direction of motion simplifies to

$$\bar{\tau}\frac{\mathrm{d}^2\hat{\zeta}}{\mathrm{d}L^2} = -(\sigma+1)\,\epsilon^2\Omega^2\hat{\zeta} + (\sigma-1)\,\epsilon^2\alpha\,\sin\bar{\theta}\frac{\mathrm{d}\hat{\zeta}}{\mathrm{d}L} + \epsilon\left(\frac{C_D}{\pi}\sin\bar{\theta} + C_N\right)\left(\mathrm{i}\Omega\hat{\zeta} + \cos\bar{\theta}\frac{\mathrm{d}\hat{\zeta}}{\mathrm{d}L}\right). \tag{2.20}$$

Once the mean geometry has been calculated, equation (2.20) can be used to determine the development of transverse vibrations. Their form is entirely independent of any oscillations in the (x, z)-plane, and is investigated in detail in §3.

Oscillations in the (x, z)-plane couple to changes in tension. In non-dimensional form equation (2.14) is

$$\frac{\mathrm{d}\hat{\xi}}{\mathrm{d}L} = \hat{\eta}\frac{\mathrm{d}\bar{\theta}}{\mathrm{d}L}, \tag{2.21}$$

For the time dependence $\mathrm{e}^{\mathrm{i}\omega t}$ equations (2.16) and (2.17) reduce to

$$\frac{\mathrm{d}\hat{\tau}}{\mathrm{d}L} = -\sigma\epsilon^2\Omega^2\hat{\xi} - (\sigma-1)\,\epsilon^2\alpha\cos\bar{\theta}\left(\frac{\mathrm{d}\hat{\eta}}{\mathrm{d}L} + \hat{\xi}\frac{\mathrm{d}\bar{\theta}}{\mathrm{d}L}\right) + \epsilon C_T\left[\mathrm{i}\Omega\hat{\xi}(1+\cos^2\bar{\theta}) - \mathrm{i}\Omega\hat{\eta}\sin\bar{\theta}\cos\bar{\theta} + \sin\bar{\theta}\left(\frac{\mathrm{d}\hat{\eta}}{\mathrm{d}L} + \hat{\xi}\frac{\mathrm{d}\bar{\theta}}{\mathrm{d}L}\right)\right], \tag{2.22}$$

and

$$\bar{\tau}\left[\frac{\mathrm{d}^2\hat{\eta}}{\mathrm{d}L^2} + \hat{\eta}\left(\frac{\mathrm{d}\bar{\theta}}{\mathrm{d}L}\right)^2\right] = -(\sigma+1)\,\epsilon^2\Omega^2\hat{\eta} + (\sigma-1)\,\epsilon^2\alpha\sin\bar{\theta}\left(\frac{\mathrm{d}\hat{\eta}}{\mathrm{d}L} - \hat{\xi}\frac{\mathrm{d}\bar{\theta}}{\mathrm{d}L}\right) - \hat{\tau}\frac{\mathrm{d}\bar{\theta}}{\mathrm{d}L} - C_T\epsilon\cos\bar{\theta}\frac{\mathrm{d}\bar{\theta}}{\mathrm{d}L}\hat{\xi} + \frac{2C_D}{\pi}\epsilon\sin\bar{\theta}\left(\mathrm{i}\Omega\hat{\eta} + \cos\bar{\theta}\frac{\mathrm{d}\hat{\eta}}{\mathrm{d}L}\right) + C_N\epsilon\left[\mathrm{i}\Omega\hat{\eta}(1+\sin^2\bar{\theta}) - \mathrm{i}\Omega\hat{\xi}\sin\bar{\theta}\cos\bar{\theta} + \cos\bar{\theta}\frac{\mathrm{d}\hat{\eta}}{\mathrm{d}L}\right]. \tag{2.23}$$

Fluctuations of the cable in the (x, z)-plane (i.e. in the vertical plane in line with the towing direction) can be determined by solution of equations (2.21)–(2.23) with appropriate boundary conditions. The form of these oscillations is discussed in §4.

3. Transverse oscillations of the cable

Transverse vibrations of the cable at a non-dimensional frequency Ω satisfy equation (2.20);

$$\bar{\tau}\frac{\mathrm{d}^2\hat{\zeta}}{\mathrm{d}L^2} = -(\sigma+1)\,\epsilon^2\Omega^2\hat{\zeta} + (\sigma-1)\,\epsilon^2\alpha\,\sin\bar{\theta}\frac{\mathrm{d}\hat{\zeta}}{\mathrm{d}L} + \epsilon\left(\frac{C_D}{\pi}\sin\bar{\theta} + C_N\right)\left(\mathrm{i}\Omega\hat{\zeta} + \cos\bar{\theta}\frac{\mathrm{d}\hat{\zeta}}{\mathrm{d}L}\right). \tag{3.1}$$

The displacement $\hat{\zeta}$ is parallel to the y-axis: that is, it is in the horizontal direction perpendicular to the mean towing velocity. This is the extension of Païdoussis' (1973) equation for a cylinder inclined at an angle to the towing direction. For a particular

frequency Ω, $\hat{\zeta}$ may be determined by an integration of (3.1) with appropriate boundary conditions at the end of the cable.

At the junction of the cable and the neutrally buoyant cylinder containing the sonar array the conditions (2.5) and (2.6) give

$$\hat{\zeta}(L_C) = Y(0), \tag{3.2}$$

and

$$\frac{d\hat{\zeta}}{dL}(L_C) = \frac{dY}{dX}(0), \tag{3.3}$$

where $L_C = l_C/l_A$ is the non-dimensional length of the cable. $Y(X)$, the displacement at a distance X along a neutrally buoyant cylinder, was determined in Part 1 equation (2.38). For such a cylinder with a free downstream end

$$Y(X) = P \sum_{n=0}^{\infty} \frac{(i\Omega b(X_c - X))^n}{n!(n+b-1)!}. \tag{3.4}$$

Since all lengths have been non-dimensionalized with respect to the cylinder length, $X_c = 1 - a_A/l_A C_T$ and $b = 2i\Omega a_A/l_A C_T + C_N/C_T$. For Re (b) greater than a half, the solution in (3.4) is valid for all positions X upstream of the critical point X_c. But when Re (b) is less than a half, it only holds in $X_c - X \gg a_A/l_A C_T$. P is an arbitrary constant to be found from the remaining boundary condition.

When the expression for $Y(X)$ in (3.4) is substituted into (3.2) and (3.3), it determines, apart from an arbitrary multiplicative constant, the values of $\hat{\zeta}$ and its derivative $d\hat{\zeta}/dL$ at the downstream end of the cable. With these two starting conditions (3.1) may be integrated from $L = L_C$ to $L = 0$ giving the transverse displacements along the cable, again apart from a scaling factor. The coefficients in (3.1) involve the mean geometry of the cable through the functions $\bar{\tau}(L)$ and $\bar{\theta}(L)$. These may be calculated by a simultaneous integration of equations (2.18) and (2.19) with the downstream boundary conditions

$$\bar{\tau}(L_C) = C_T a_A/l_A, \quad \bar{\theta}(L_C) = 0, \tag{3.5a, b}$$

the non-dimensional form of (2.9) and (2.10)

Equations (3.1), (2.18) and (2.19) were integrated numerically from the downstream end of the cable to its upstream end using a Runge–Kutta–Merson method. This determines directly the form of transverse oscillations of the cable of frequency Ω. Vibration of the neutrally buoyant cylinder is described by (3.4). The scaling constant P may be found from the boundary condition at the upstream end of the cable. For example, in an investigation of the response of a cable and towed array to ship manoeuvres, the amplitudes of the transverse displacement at the upstream end of the cable would be known.

Before investigating the forced response of a towed cable and cylinder, it is important to determine whether they are stable when towed at a constant velocity. Then there is no perturbation at the upstream end of the cable, so that

$$\hat{\zeta}(0) = 0. \tag{3.6}$$

The eigenfrequencies Ω may be determined by a numerical integration of (3.1) with a subsequent iteration in Ω to find frequencies that satisfy (3.6). If all the roots Ω have positive imaginary part, the eigenmodes decay with time and the system is stable. A root in the lower half Ω-plane means that an eigenmode grows in time and the towed cable and cylinder are unstable.

The stability of the towed cable and cylinder has been investigated numerically for a cylinder with $a_A = 8.25 \times 10^{-5} l_A$, $gl_A/U^2 = 578$ and a cable of dimensions $l_C = 3.7 l_A$, $a_C = 4.125 \times 10^{-5} l_A$, $\sigma = 2.8$ with drag coefficients $C_T = 0.0025$, $C_D = 1.2$ and two values of C_N; $C_N = 0.25 C_T$ and $C_N = 0.75 C_T$. The contours $\mathrm{Re}\,\hat{\zeta}(0) = 0$ and $\mathrm{Im}\,\hat{\zeta}(0) = 0$ have been plotted in the lower half Ω-plane. They do not intersect demonstrating that there are no eigenfrequencies with negative imaginary part. Hence the towed cable and cylinder are stable to transverse perturbations.

It is therefore appropriate to investigate the response of the cable and cylinder to forcing. We consider the towing ship to follow a meandering track at a frequency ω and, without loss of generality, take the non-dimensional amplitude of this vibration to be unity, so that

$$\hat{\zeta}(0) = 1. \tag{3.7}$$

This boundary condition together with the downstream-end conditions (3.2) and (3.3), and equation (3.1) completely specify the transverse displacement of the cable. The vibration of the cylinder is described by (3.4). The magnitude and phase of this transverse displacement is plotted in figure 3 for three different values of Ω and the same cylinder and cable geometry, i.e. $a_A = 8.25 \times 10^{-5} l_A$, $gl_A/U^2 = 578$, $l_C = 3.7 l_A$, $a_C = 4.125 \times 10^{-5} l_A$, $\sigma = 2.8$, $C_T = 0.0025$, $C_N = 0.75 C_T$, $C_D = 1.2$. Before discussing the graphs it is appropriate to investigate the low- and high-frequency limits analytically where simple forms for $\hat{\zeta}(L)$ can be derived.

The mean cable inclination is constant over most of its length and equal to the critical angle $\bar{\theta}_c$. In this range the mean cable parameters simplify and (3.1) leads to an easier equation for $\hat{\zeta}(L)$. Let us suppose that $\theta = \bar{\theta}_c$ is a good approximation to the actual cable position over a non-dimensional length L_0. The increase in mean cable tension is described by (2.18),

$$\frac{\mathrm{d}\bar{\tau}}{\mathrm{d}L} = -(\sigma - 1)\,\epsilon^2 \alpha \sin\bar{\theta} - \epsilon C_T \cos\bar{\theta}.$$

In the range $0 \leqslant L \leqslant L_0$, this first-order differential equation has constant coefficients and can be readily integrated to give

$$\bar{\tau}(L) = \bar{\tau}(L_0) + [(\sigma - 1)\,\epsilon^2 \alpha \sin\bar{\theta}_c + \epsilon C_T \cos\bar{\theta}_c](L_0 - L). \tag{3.8}$$

When this is substituted into (3.1) it shows that $\hat{\zeta}(L)$ satisfies

$$(L_1 - L)\frac{\mathrm{d}^2\hat{\zeta}}{\mathrm{d}L^2} - f\frac{\mathrm{d}\hat{\zeta}}{\mathrm{d}L} + h\hat{\zeta} = 0 \quad \text{for} \quad 0 \leqslant L \leqslant L_0, \tag{3.9}$$

where

$$L_1 = L_0 + \frac{\bar{\tau}(L_0)}{(\sigma - 1)\,\epsilon^2 \alpha \sin\bar{\theta}_c + \epsilon C_T \cos\bar{\theta}_c}, \tag{3.10a}$$

$$f = \frac{(\sigma - 1)\,\epsilon\alpha \sin\bar{\theta}_c + (C_N + C_D \sin\bar{\theta}_c/\pi)\cos\bar{\theta}_c}{(\sigma - 1)\,\epsilon\alpha \sin\bar{\theta}_c + C_T \cos\bar{\theta}_c}, \tag{3.10b}$$

and

$$h = \frac{(\sigma + 1)\,\epsilon\Omega^2 - \mathrm{i}\Omega(C_N + C_D \sin\bar{\theta}_c/\pi)}{(\sigma - 1)\,\epsilon\alpha \sin\bar{\theta}_c + C_T \cos\bar{\theta}_c}, \tag{3.10c}$$

L_1, f and h are all independent of position L. When C_N is set equal to zero and the gravity term $(\sigma - 1)\,\epsilon\alpha \sin\bar{\theta}_c$ is neglected, (3.9) reduces to the form given by Lyon (1962, equations (2.9) and (2.23)) for perturbations of a string with a linear variation in tension.

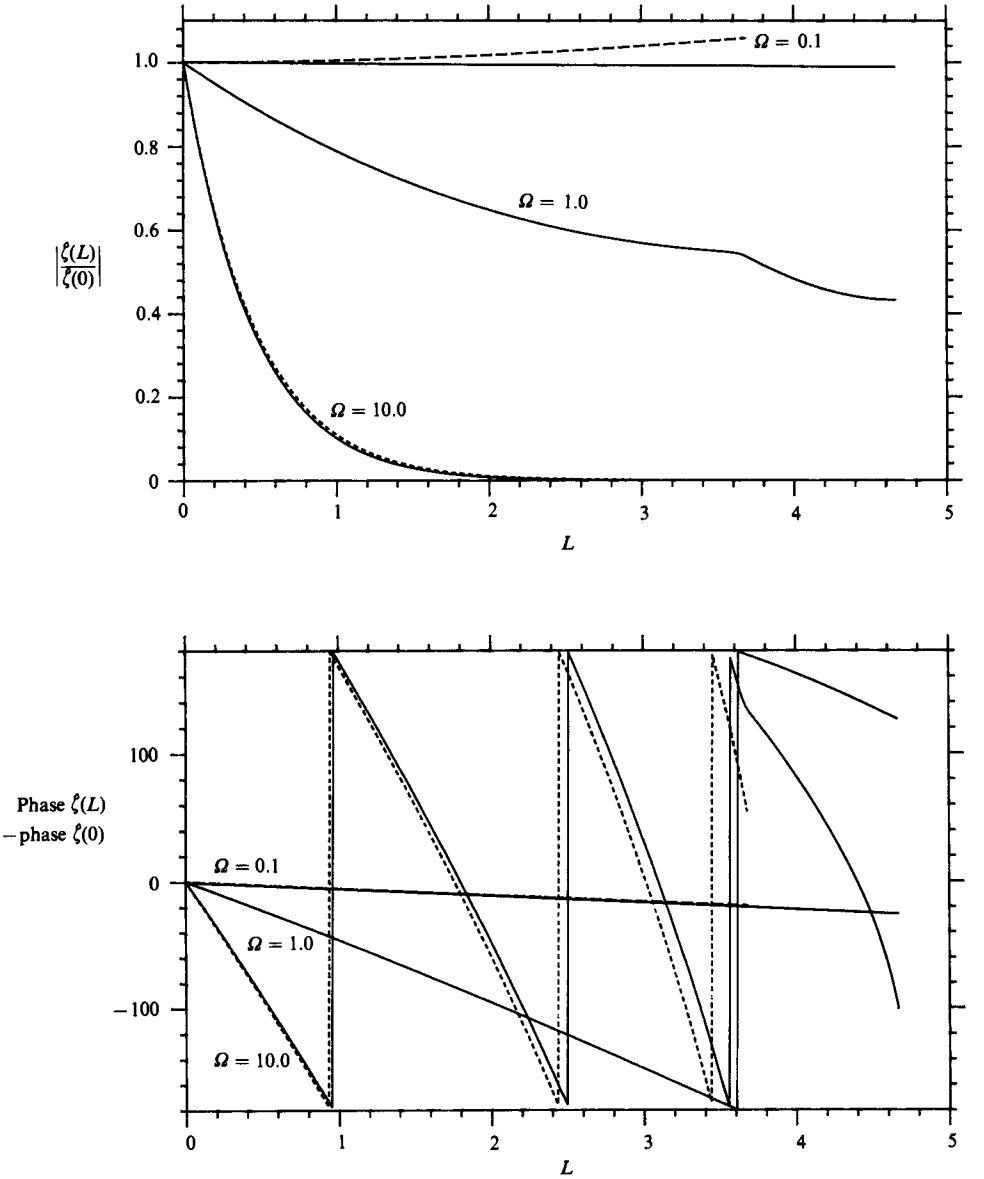

FIGURE 3. Plots of the variation in the magnitude and phase of the transverse displacement with distance along the cable and cylinder for three values of Ω. The cable and cylinder parameters are as in figure 2. The cylinder extends from $L = 3.7$ to $L = 4.7$. ——, low-frequency asymptotic form (equation (3.13)); ------, high-frequency asymptotic form (equation (3.20)).

The low-frequency behaviour of $\hat{\zeta}(L)$ may be investigated conveniently by evaluating the series solutions of (3.9). Then $\hat{\zeta}(L)$ is expressed as

$$\hat{\zeta}(L) = (L_1 - L)^{\gamma} \sum_{n=0}^{\infty} \beta_n (L_1 - L)^n,$$

and substituted into (3.9). The indicial equation has two roots, which are $\gamma = 0$ and $1-f$. The coefficients β_n are found to satisfy the recurrence relationship

$\beta_n = -\beta_{n-1}h/(n+\gamma)(n+\gamma+f-1)$. At low frequencies the terms in these series decrease rapidly with n, and only the first few need to be retained. This leads to an approximate form for the general solution

$$\hat{\zeta}(L) = R_1\left\{1-\frac{h(L_1-L)}{f}+\ldots\right\}+S_1(L_1-L)^{1-f}\left\{1-\frac{h(L_1-L)}{2-f}+\ldots\right\}, \tag{3.11}$$

in the range $0 \leqslant L \leqslant L_0$. This truncation of the infinite series is a good approximation for frequencies sufficiently low to ensure that $|h/f|$ is small in comparison with unity. The two constants R_1 and S_1 are determined precisely by boundary conditions at $L = 0$ and L_0. But calculation of $\hat{\zeta}(L_0)$ requires a numerical integration of (3.1) over a region near the downstream end of the cable where $\bar{\theta}$ varies rapidly. An approximate analytical solution can be obtained by noting that the boundary condition at $\hat{\zeta}(L_0)$ will in general lead to

$$S_1 \sim R_1(L_1-L_0)^{f-1}.$$

For typical cable parameters f is a large positive constant and so $S_1(L_1-L)^{1-f}$ is small once L is appreciably smaller than L_0. Equation (3.11) therefore simplifies to

$$\hat{\zeta}(L) \approx R_1\left\{1-\frac{h(L_1-L)}{f}+\ldots\right\} \tag{3.12}$$

over the range $0 \leqslant L \ll L_0$. The value of R_1 then follows immediately from the upstream boundary condition $\hat{\zeta}(0) = 1$. Hence we conclude that

$$\hat{\zeta}(L) \sim 1+hL/f, \tag{3.13}$$

describes the low-frequency displacements of most of the cable. This approximate form is plotted in figure 3 for comparison with the exact solution obtained numerically. It gives a good prediction of the phase of the low-frequency disturbance, its amplitude being approximately unity.

A high-frequency asymptotic solution can be obtained by making a WKB approximation. First a new variable $W(Z)$ is introduced to reduce the differential equation to standard form. With $\hat{\zeta}(L) = Z^{-\frac{1}{2}f}W(Z)$ and $Z = L_1-L$, equation (3.9) reduces to

$$W''+qW = 0, \tag{3.14}$$

where the dash denotes a derivative and

$$q(Z) = \frac{h}{Z}-\frac{f}{4Z^2}(f-2). \tag{3.15}$$

In the usual way we look for solutions of the form

$$W(Z) = A(Z)\,\mathrm{e}^{\mathrm{i}\Theta(Z)}, \tag{3.16}$$

and choose

$$\Theta(Z) = \pm\int^Z q^{\frac{1}{2}}(\tilde{Z})\,\mathrm{d}\tilde{Z}. \tag{3.17}$$

At high frequencies the 'amplitude' A varies slowly in comparison with the 'phase' term Θ. The essence of the WKB method is to neglect A'' in comparison with $A'\Theta'$. This approximation leads to a first-order equation for $A(Z)$, which can be integrated immediately to give

$$A(Z) = q^{-\frac{1}{4}}. \tag{3.18}$$

It is now possible to substitute back and see when $A''/A'\Theta'$ is small. This shows that the solution is valid whenever $|hZ|$ is large, i.e. for $|\Omega|$ much greater than unity.

For large $|hZ|$, $q(Z)$ can be simplified to h/Z. Then $\Theta(Z) = \pm 2h^{\frac{1}{2}}Z^{\frac{1}{2}}$, $A(Z) = h^{-\frac{1}{4}}Z^{\frac{1}{4}}$, and so the asymptotic high-frequency solution is

$$\hat{\zeta}(L) = h^{-\frac{1}{4}}(L_1-L)^{\frac{1}{4}-\frac{1}{2}f}\{R_2\exp[2\mathrm{i}h^{\frac{1}{2}}(L_1-L)^{\frac{1}{2}}]+S_2\exp[-2\mathrm{i}h^{\frac{1}{2}}(L_1-L)^{\frac{1}{2}}]\}, \quad (3.19)$$

for $0 \leqslant L \leqslant L_0$. The root of $h^{\frac{1}{2}}$ is chosen so that it has negative imaginary part.

Again the constants R_2 and S_2 are determined exactly by boundary conditions at $L = 0$ and L_0. But for the purposes of obtaining an approximate solution, we note that the boundary conditions at $L = L_0$ will lead to

$$S_2 \sim R_2\exp[4\mathrm{i}h^{\frac{1}{2}}(L_1-L_0)^{\frac{1}{2}}].$$

This means that when L is appreciably less than L_0 the second term in (3.19) will be much smaller than the first. Hence

$$\hat{\zeta}(L) \simeq h^{-\frac{1}{4}}(L_1-L)^{\frac{1}{4}-\frac{1}{2}f}R_2\exp[2\mathrm{i}h^{\frac{1}{2}}(L_1-L)^{\frac{1}{2}}], \quad (3.20)$$

for $0 \leqslant L \ll L_0$. The value of the constant R_2 then follows immediately from the upstream boundary condition to give

$$\hat{\zeta}(L) = (1-L/L_1)^{\frac{1}{4}-\frac{1}{2}f}\exp[-2\mathrm{i}h^{\frac{1}{2}}\{L_1^{\frac{1}{2}}-(L_1-L)^{\frac{1}{2}}\}]. \quad (3.21)$$

This approximate asymptotic form is sketched in figure 3 for the large non-dimensional frequency $\Omega = 10$. It is in good agreement with the exact solution.

Figure 3 shows the phase speed of the moderate and low-frequency disturbances to be of order unity. In terms of dimensional parameters this means that disturbances propagate down the cable with a phase speed comparable with the towing speed. Ketchman's (1981) approximate method of determining the vibration of an inclined cable is therefore inappropriate for this frequency range. Since he assumes that disturbances travel at the faster speed $(T/\rho_0\sigma\pi a_C^2)^{\frac{1}{2}}$ to obtain their amplitude by an energy argument.

To summarize, low-frequency disturbances propagate along the cable with little attenuation, while the amplitude of high-frequency disturbances is significantly reduced as they travel down the cable. The cable acts as an effective low-pass filter.

The actual form of the transverse displacement of the cable is of limited interest. What is relevant is how much vibration is transmitted along the cable from the towing ship to the cylinder containing the sonar array. This is described by the ratio $\mathbb{T} = \hat{\zeta}(L_C)/\hat{\zeta}(0)$. Since the displacements of the cable and cylinder are equal at their junction (boundary condition (3.2)), $\zeta(L_C)$ is the same as the displacement of the leading edge of the cylinder. In Part 1 the transverse vibration of the cylinder was given in terms of the motion of its leading edge. The transfer function $\mathbb{T}$ and the result of Part 1 are therefore all that is needed for a complete description of the array motion in terms of the ship's path.

In Part 1 the value of the normal drag coefficient C_N was found to have a considerable influence on the propagation of disturbances along the array. The cable is different. Since it is negatively buoyant and inclined at an angle to the flow, its normal drag is mainly proportional to $C_D\sin\bar{\theta}$ which is much larger than C_N. Figure 4 shows the transfer coefficient $\mathbb{T}$ to be virtually independent of C_N, which is reassuring in view of the uncertainty in the value of C_N.

It is appropriate to investigate how the cable parameters influence this transfer

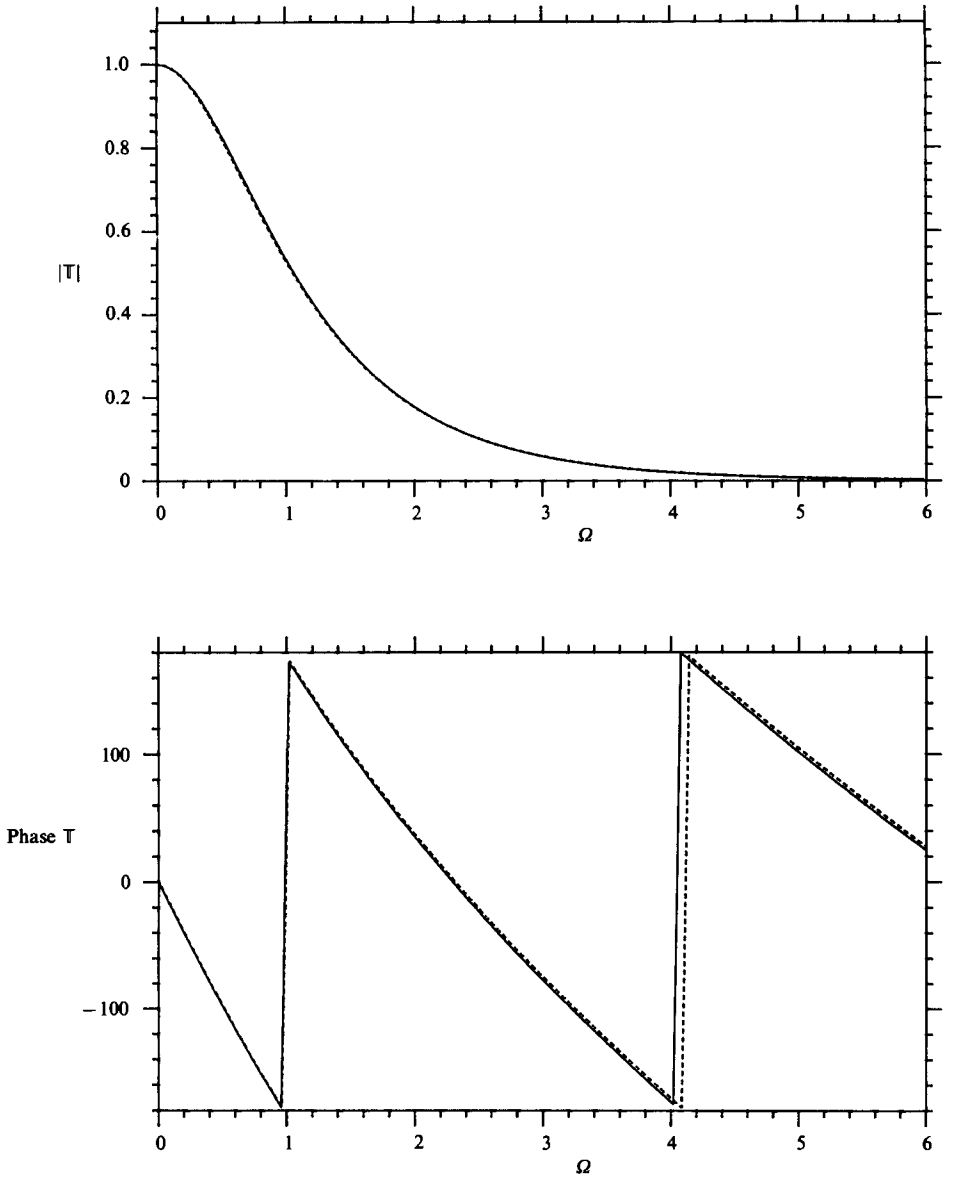

FIGURE 4. The effect of changes in C_N on the transfer of transverse oscillations along the cable. The other cable and cylinder parameters are as in figure 2. -----, $C_N = 0.25C_T$; ——, $C_N = 0.75C_T$.

function. It is not surprising that $\mathbb{T}$ is found to depend strongly on a non-dimensional frequency $\tilde{\Omega}$, with

$$\tilde{\Omega} = \Omega L_C, \tag{3.22}$$

or in terms of the dimensional frequency ω

$$\tilde{\Omega} = \omega l_C / U. \tag{3.23}$$

Figures 5–8 show the effect of varying the cable parameters for a given cylinder geometry and fixed drag coefficients. In these diagrams $a_A = 8.25 \times 10^{-5} l_A$, $C_T = 0.0025$, $C_N = 0.75C_T$ and $C_D = 1.2$.

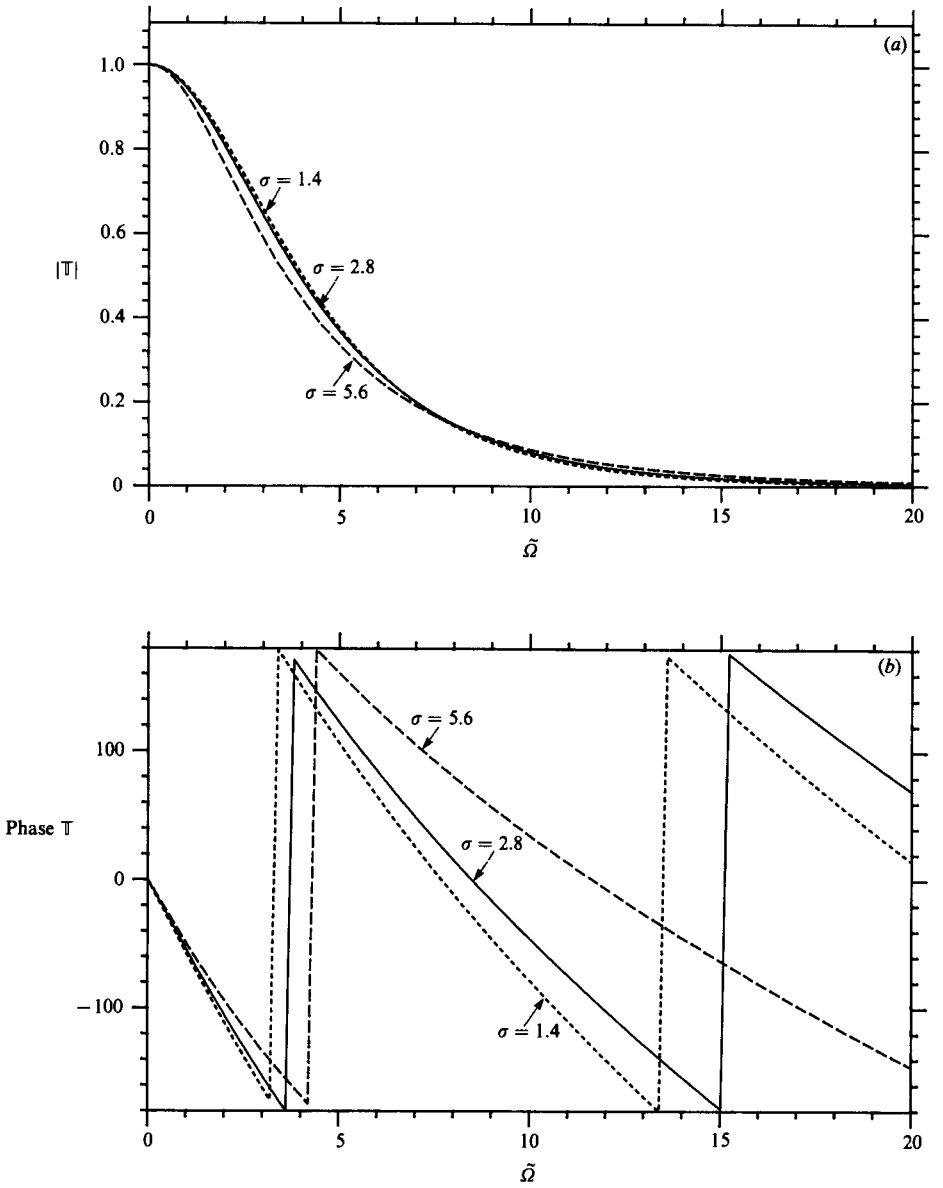

FIGURE 5(*a*, *b*). For caption see page 548.

Figure 5 shows the effect of changes in σ, the specific density of the cable. It demonstrates that variations in the density of a negatively buoyant cable only have a slight effect on the amplitude of the disturbances transmitted down the cable, with a heavier cable producing slightly more attenuation at lower frequencies and less at higher frequencies than a lighter cable. The phase of the transfer function is plotted in figure 5(*b*) as a function of $\tilde{\Omega}$. The slope of the curves shows that at low and moderate frequencies the disturbances propagate down the cable with a phase speed of the order of the towing speed, travelling slightly faster along the heavier cable. The phase speed is faster for higher frequencies. A comparison of figure 5(*a*) and (*c*) shows that a heavier-than-water cable produces less attenuation at low frequencies

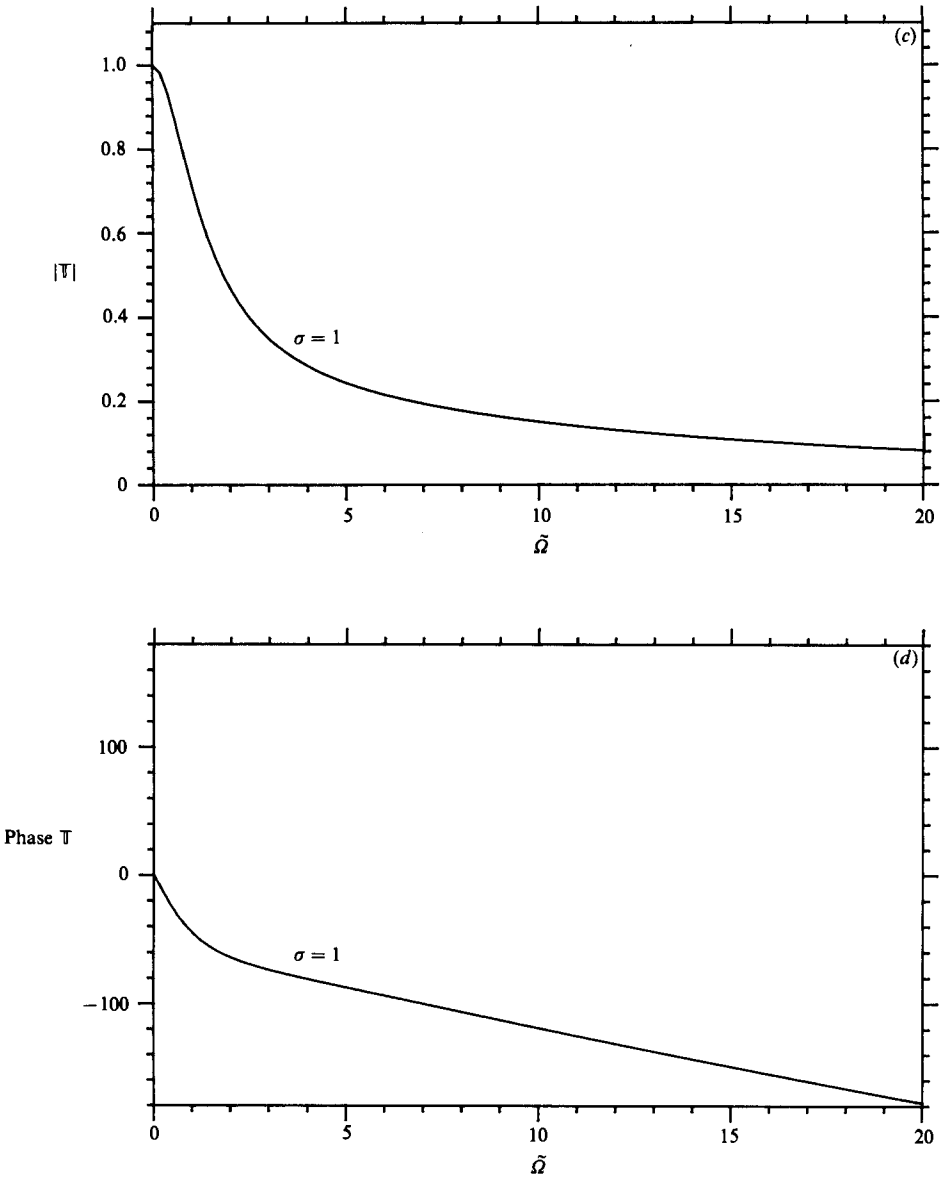

FIGURE 5. The effect of changes in σ, the specific density of the cable, on the transfer of transverse oscillations along the cable. $l_C/l_A = 3.7$, $gl_A/U^2 = 578$, $a_C/l_A = 4.125 \times 10^{-5}$ and $a_A/l_A = 8.25 \times 10^{-5}$, $C_T = 0.0025$, $C_N = 0.75C_T$ with $C_D = 1.2$.

than a neutrally buoyant cable of the same length, but more at high frequencies. The cross-over occurs at a non-dimensional frequency, $\tilde{\Omega}$, of about 7.

The effect of altering the cable length l_C is shown in figure 6. Again the three curves are very close, demonstrating that the transfer function at fixed $\tilde{\Omega}$ is only slightly modified by significant changes in l_C. The abscissa $\tilde{\Omega} = \omega l_C/U$ is also a function of l_C. It accounts for the main effect of changes in cable length on the transmission of disturbances of a given dimensional frequency ω along the cable. For a fixed value of ω, increasing l_C increases $\tilde{\Omega}$ and enhances the attenuation produced by the cable. Conversely, a shorter cable produces less attenuation.

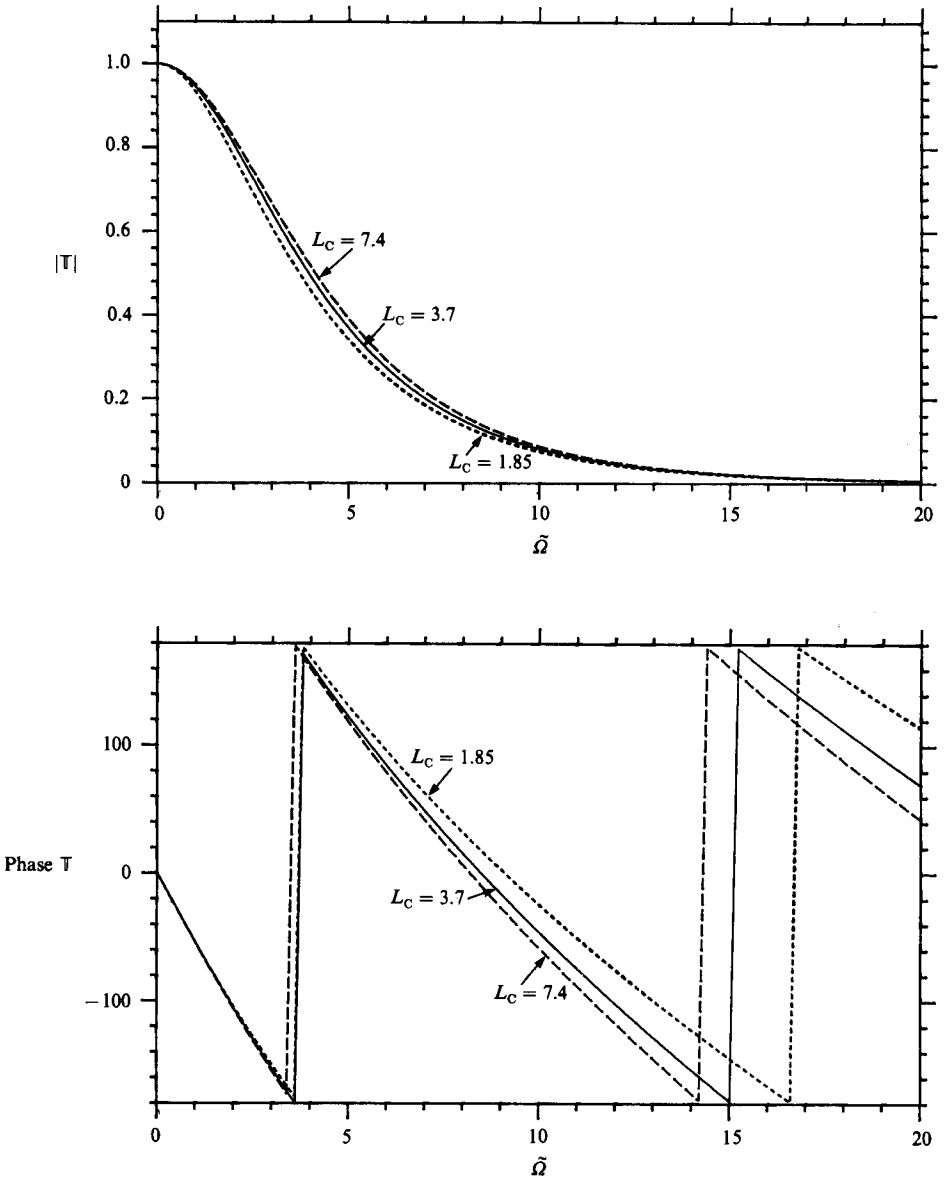

FIGURE 6. The effect of changes in $L_C = l_C/l_A$, the non-dimensional length of the cable, on the transfer of transverse oscillations along the cable. $\sigma = 2.8$, $gl_A/U^2 = 578$, $a_C/l_A = 4.125 \times 10^{-5}$. The cylinder geometry and drag coefficients are as in figure 5.

Figure 7 shows the effect of changes in the Froude number. The three curves show that at a fixed $\tilde{\Omega}$ there is little effect even when the towing velocity is doubled or halved. Again the main dependence is described through the variation of $\tilde{\Omega}$ with U. For a fixed frequency ω, an increase in the towing speed, U, decreases $\tilde{\Omega}$ and the attenuation across the cable is reduced. Figure 8 shows that the cable diameter only has a weak effect.

Kennedy & Strahan (1981) measured the transmission loss across a cable towing an array. Their data is reproduced in table 1 and provides an appropriate test for this

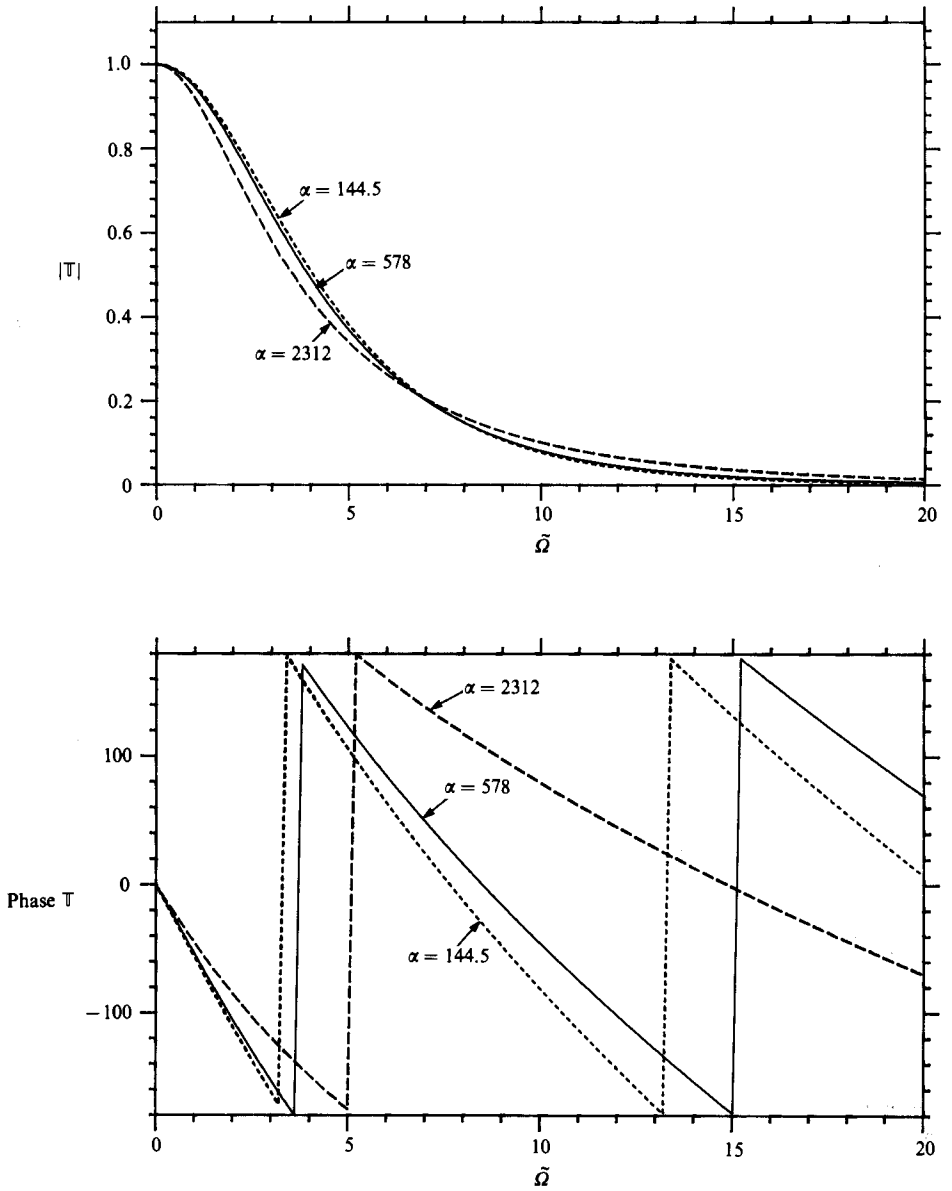

FIGURE 7. The effects of changes in $\alpha = gl_A/U^2$, the inverse-square Froude number, on the transfer of transverse oscillations along the cable. $\sigma = 2.8$, $l_C/l_A = 3.7$, $a_C/l_A = 4.125 \times 10^{-5}$. The cylinder geometry and drag coefficients are as in figure 5.

theory. They choose to express the phase of $\mathbb{T}$ in terms of a parameter c^* defined by

$$c^* = -\frac{\tilde{\Omega}}{\arg \mathbb{T}}. \tag{3.24}$$

For consistency the same notation is adopted here. The argument of $\mathbb{T}$ is multivalued making c^* multivalued too. The results in figures 5–8 suggest that the argument of $\mathbb{T}$ in radians is greater than $-\tilde{\Omega}$. This has been used in the presentation of the

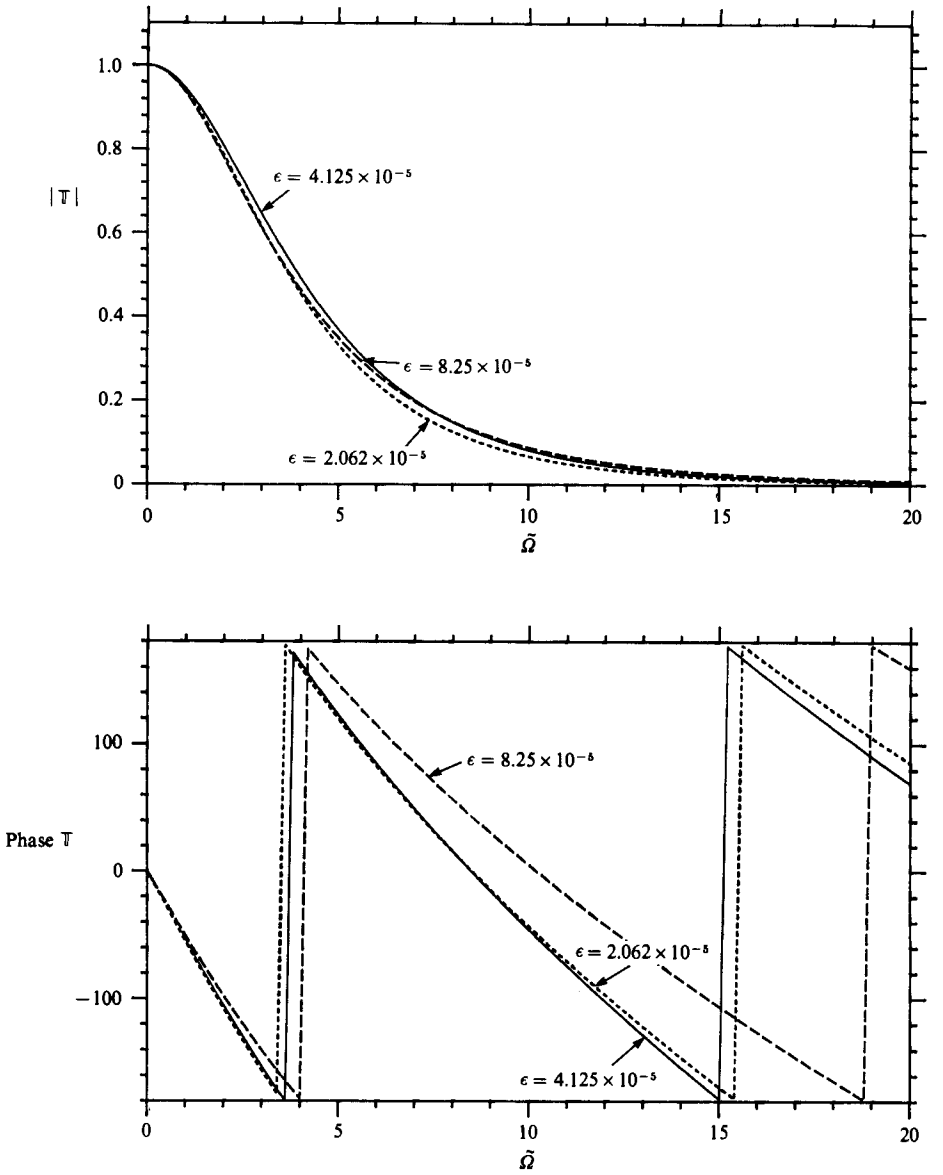

FIGURE 8. The effects of changes in cable radius, $\epsilon = a_C/l_A$, on the transfer of transverse oscillations along the cable. $\sigma = 2.8$, $l_C/l_A = 3.7$, $gl_A/U^2 = 578$. The cylinder geometry and drag coefficients are as in figure 5.

theoretical results by, somewhat arbitrarily, choosing the branch of arg $\mathbb{T}$ such that

$$2\pi - \tilde{\Omega} > \arg \mathbb{T} > -\tilde{\Omega}. \tag{3.25}$$

Satisfactory comparison with the experimental data suggests that this is also the branch chosen by Kennedy & Strahan. They used a 16 mm steel cable, and so the theoretical curves in figure 9 are for $a_C = 8$ mm, $\sigma = 7.8$ and a range of values of U and l_C. But, as demonstrated, by figures 6 and 7 such changes in velocity and cable length only lead to small changes in the transfer function $\mathbb{T}$ at fixed $\tilde{\Omega}$. Lowering the speed or shortening the cable increases the attenuation at moderate values of Ω. The

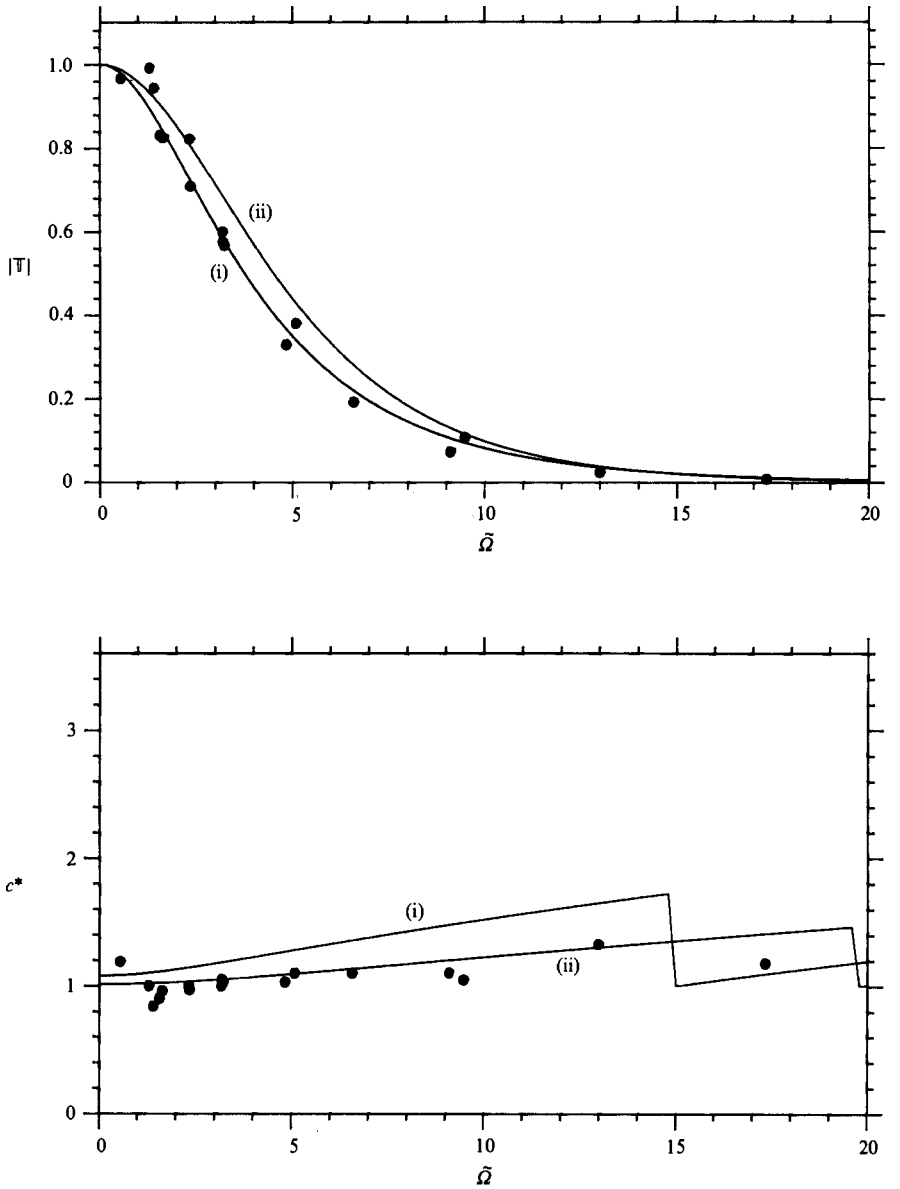

FIGURE 9. Comparison of theory and experiment. $\sigma = 7.8$, $a_C = 8$ mm, $C_T = 0.0025$, $C_D = 1.2$, $C_N = 0.75C_T$. ●, experimental data (Kennedy & Strahan 1981).

theoretical curves in figure 9 are for the two extreme cases in the experimental data. Curve (i) is for the lowest experimental speed and the shortest length of cable, while curve (ii) is for the highest experimental speed and the longest cable length. For perfect agreement all the experimental points should lie between these two theoretical curves, and indeed this is nearly satisfied.

Kennedy & Strahan compared their experimental results with a simple theory in which they solve the equation for a neutrally buoyant cable. One effect of negative buoyancy is that the cable is inclined at a finite angle to the towing direction and,

l_c (m)	U (m/s)	$\omega/2\pi$ (mHz)	$\lvert\mathbb{T}\rvert$	c^*
1186.9	3.10	0.97	0.8223	1.00
1186.4	3.03	2.07	0.3804	1.10
1186.0	2.98	3.79	0.1075	1.05
1185.7	2.94	6.84	0.0085	1.18
1193.8	5.10	0.37	0.9671	1.19
1194.1	5.25	1.10	0.8313	0.90
1193.9	5.18	2.20	0.6004	1.00
1193.5	5.00	4.39	0.1922	1.10
1192.6	4.72	8.18	0.0243	1.33
1196.0	6.35	1.10	0.9916	1.00
1195.9	6.25	1.96	0.7091	0.97
1195.9	6.26	4.03	0.3293	1.03
1196.1	6.45	7.81	0.0727	1.10
1193.9	5.15	0.97	0.9442	0.84
1193.8	5.10	2.20	0.5683	1.03
597.1	5.28	2.32	0.8255	0.96
596.9	5.15	4.39	0.5759	1.05

TABLE 1. Kennedy & Strahan's experimental results

as shown by equation (2.2*b*), experiences a considerably larger normal force than a similar neutrally buoyant cable. Kennedy & Strahan attempt to include this aspect of negative buoyancy by using an artificially large value of C_N in their equation for a neutrally buoyant cable. The value of C_N was adjusted to fit the data. They found that a certain value of C_N gave good agreement between measured and calculated amplitudes, but a different C_N was required for the phases to agree. No such empirical fit has been made in the results presented here. The values of the drag coefficients have been chosen on physical grounds, and so the correlation between theory and experiment is encouraging.

Having demonstrated that the theoretical description of vibrations in a horizontal plane is in reasonable agreement with measurements we will go on to consider oscillations in a vertical plane.

4. Vertical oscillations of the cable

When the cable vibrates in the (x, z)-plane, normal and longitudinal cable displacements couple and are influenced by changes in tension. Small changes in the ship's speed provide a forcing mechanism for these oscillations, since unsteady ship motion produces fluctuations in the horizontal position of the upstream end of the cable. These disturbances propagate down the cable and, as we will see, can cause significant horizontal and vertical displacements of the neutrally buoyant cylinder containing the sonar array.

The tangential cable displacement at a non-dimensional length L along the cable, $\hat{\xi}(L)$, is related to its normal displacement in the (x, y)-plane by equation (2.21);

$$\frac{\mathrm{d}\hat{\xi}}{\mathrm{d}L} = \hat{\eta}\frac{\mathrm{d}\bar{\theta}}{\mathrm{d}L}. \tag{4.1}$$

Fluctuations in $\hat{\tau}(L)$, the non-dimensional cable tension, are related to the in-plane displacements by (2.22)

$$\frac{\mathrm{d}\hat{\tau}}{\mathrm{d}L} = -\sigma\Omega^2\epsilon^2\hat{\xi} - (\sigma-1)\,\epsilon^2\alpha\cos\bar{\theta}\left(\frac{\mathrm{d}\hat{\eta}}{\mathrm{d}L} + \hat{\xi}\frac{\mathrm{d}\bar{\theta}}{\mathrm{d}L}\right) + \epsilon C_{\mathrm{T}}\left[\mathrm{i}\Omega\hat{\xi}(1+\cos^2\bar{\theta})\right.$$
$$\left. - \mathrm{i}\Omega\hat{\eta}\sin\bar{\theta}\cos\bar{\theta} + \sin\bar{\theta}\left(\frac{\mathrm{d}\hat{\eta}}{\mathrm{d}L} + \hat{\xi}\frac{\mathrm{d}\bar{\theta}}{\mathrm{d}L}\right)\right], \quad (4.2)$$

while $\hat{\eta}(L)$ satisfies the second-order differential equation (2.23)

$$\bar{\tau}\left[\frac{\mathrm{d}^2\hat{\eta}}{\mathrm{d}L^2} + \hat{\eta}\left(\frac{\mathrm{d}\bar{\theta}}{\mathrm{d}L}\right)^2\right] = -(\sigma+1)\,\epsilon^2\Omega^2\hat{\eta} + (\sigma-1)\,\epsilon^2\alpha\sin\bar{\theta}\left(\frac{\mathrm{d}\hat{\eta}}{\mathrm{d}L} - \hat{\xi}\frac{\mathrm{d}\bar{\theta}}{\mathrm{d}L}\right)$$
$$- \hat{\tau}\frac{\mathrm{d}\bar{\theta}}{\mathrm{d}L} - C_{\mathrm{T}}\,\epsilon\cos\bar{\theta}\frac{\mathrm{d}\bar{\theta}}{\mathrm{d}L}\hat{\xi} + \frac{2C_{\mathrm{D}}}{\pi}\,\epsilon\sin\bar{\theta}\left(\mathrm{i}\Omega\hat{\eta} + \cos\bar{\theta}\frac{\mathrm{d}\hat{\eta}}{\mathrm{d}L}\right)$$
$$+ C_{\mathrm{N}}\,\epsilon\left[\mathrm{i}\Omega\hat{\eta}\,(1+\sin^2\bar{\theta}) - \mathrm{i}\Omega\hat{\xi}\sin\bar{\theta}\cos\bar{\theta} + \cos\bar{\theta}\frac{\mathrm{d}\hat{\eta}}{\mathrm{d}L}\right]. \quad (4.3)$$

For a particular frequency Ω, the oscillations of the cable in the (x, y)-plane may be determined by an integration of equations (4.1)–(4.3) with appropriate boundary conditions at the end of the cable.

The downstream end of the cable is attached to the cylinder, and boundary conditions (2.5) and (2.6) state that the displacement and tension force are to be continuous across this junction i.e.

$$[\boldsymbol{r}'(l_{\mathrm{C}}, t)]^{\text{cable}}_{\text{cylinder}} = \mathbf{0}, \quad (4.4)$$

$$[\boldsymbol{s}(l_{\mathrm{C}}, t)]^{\text{cable}}_{\text{cylinder}} = \mathbf{0}, \quad (4.5)$$

and

$$[T'(l_{\mathrm{C}}, t)]^{\text{cable}}_{\text{cylinder}} = 0. \quad (4.6)$$

$\hat{\eta}(L_{\mathrm{C}})$ is the complex amplitude of the normal displacement at the end of the cable. Hence it follows from (4.4) that

$$\hat{\eta}(L_{\mathrm{C}}) = Y(0). \quad (4.7)$$

$Y(X)$, the normal displacement a non-dimensional distance X along the cylinder, has been evaluated in Part 1 equation (2.38) and is given by

$$Y(X) = P\sum_{n=0}^{\infty}\frac{(\mathrm{i}\Omega b(X_{\mathrm{c}}-X))^n}{n!\,(n+b-1)!}. \quad (4.8)$$

All lengths have been non-dimensionalized with respect to the cylinder length, and so $X_{\mathrm{c}} = 1 - a_{\mathrm{A}}/l_{\mathrm{A}}C_{\mathrm{T}}$, $b = 2\mathrm{i}\Omega a_{\mathrm{A}}/l_{\mathrm{A}}C_{\mathrm{T}} + C_{\mathrm{N}}/C_{\mathrm{T}}$. P is an arbitrary constant to be determined from the boundary conditions.

The tangential direction at the cable end is given by (A 5) and (A 6) with $\bar{\theta} = 0$. Hence the boundary condition (4.5) is equivalent to

$$\frac{\mathrm{d}\hat{\eta}}{\mathrm{d}L}(L_{\mathrm{C}}) + \hat{\xi}\frac{\mathrm{d}\bar{\theta}}{\mathrm{d}L}(L_{\mathrm{C}}) = \frac{\mathrm{d}Y}{\mathrm{d}X}(0). \quad (4.9)$$

The tangential component of (4.4) shows that an in-line displacement of the downstream end of the cable results in a corresponding displacement of the cylinder and towed array. Equations (4.1) and (4.2) were derived with the cable in mind, but

they can be applied equally well to the neutrally buoyant cylinder provided we put $L = X$, $\sigma = 1$, $\bar{\theta} \equiv 0$ and $\epsilon = \epsilon_A = a_A/l_A$. The cylinder has a simple mean geometry: it is straight and horizontal. This enables these equations to be integrated immediately. Equation (4.1) shows that $\hat{\xi}$ is constant along the cylinder while (4.2) describes the linear increase in the amplitude of the unsteady tension along the cylinder. It shows that at the leading edge of the cylinder

$$\hat{\tau} = (\Omega^2 \epsilon_A^2 - 2i\Omega\epsilon_A C_T)\hat{\xi}. \tag{4.10}$$

A third downstream boundary condition for the cable then follows from (4.4) and (4.6) and is

$$\hat{\tau}(L_C) = (\Omega^2 \epsilon_A^2 - 2i\Omega\epsilon_A C_T)\hat{\xi}(L_C). \tag{4.11}$$

The upstream end of the cable is assumed to be always on the sea-surface $z = 0$. Hence

$$\hat{\xi} \sin\bar{\theta} + \hat{\eta} \cos\bar{\theta} = 0 \quad \text{at } L = 0, \tag{4.12}$$

and in a particular problem the horizontal displacement of the cable at the towing point will be given, i.e.

$$\hat{\xi} \cos\bar{\theta} - \hat{\eta} \sin\bar{\theta} \quad \text{is specified at } L = 0. \tag{4.13}$$

For a particular non-dimensional frequency Ω, equations (4.1)–(4.3), with boundary conditions (4.7), (4.9), (4.11)–(4.13), specify a mixed boundary value problem for the in-plane cable deflections. This can be solved in a straight-forward way by numerical integration of the equations.

Before discussing the forced response of the cable we will investigate the free modes to see whether the cable and cylinder are stable under constant towing conditions. A constant towing velocity means no perturbation in the position of the upstream end of the cable, and so

$$\hat{\xi} \cos\bar{\theta} - \hat{\eta} \sin\bar{\theta} = 0 \quad \text{at } L = 0. \tag{4.14}$$

The eigenfrequencies are the values of Ω for which (4.14) is satisfied. If all these roots have positive imaginary part, all the eigenmodes decay in time and the cable and cylinder are stable to towing. If however one or more of the roots of (4.14) lie in the lower half Ω-plane, disturbances grow in time and the cable and cylinder are unstable.

The eigenfrequencies have been investigated numerically for the usual geometry; $a_A = 8.25 \times 10^{-5} l_A$, $gl_A/U^2 = 578$ and a cable of dimensions $l_C = 3.7 l_A$, $a_C = 4.125 \times 10^{-5} l_A$, $\sigma = 2.8$ with drag coefficients $C_T = 0.0025$, $C_D = 1.2$ and two values for C_N; $C_N = 0.25 C_T$ and $C_N = 0.075 C_T$. The contours $\mathrm{Re}\,(\hat{\xi}(0)\cos\bar{\theta} - \hat{\eta}(0)\sin\bar{\theta}) = 0$ and $\mathrm{Im}\,(\hat{\xi}(0)\cos\bar{\theta} - \hat{\eta}(0)\sin\bar{\theta}) = 0$ have been plotted in the lower half Ω-plane. They do not intersect and so there are no eigenfrequencies with negative imaginary part. The towed cable and cylinder are therefore stable to in-plane perturbations.

Since the cable and cylinder are stable it is appropriate to investigate their response to forcing. We consider the ship to be in unsteady motion in the negative x-direction with the ship's speed having a small perturbation about its mean value U. For a linear perturbation the response at each frequency ω may be analysed separately. Also, since the perturbation equations are linear, the non-dimensional amplitude of the displacement of the towing point may, without loss of generality, be taken to be unity, making the boundary condition (4.13)

$$\hat{\xi} \cos\bar{\theta} - \hat{\eta} \sin\bar{\theta} = 1 \quad \text{at } L = 0. \tag{4.15}$$

The two upstream conditions (4.12) and (4.15) combine to give

$$\hat{\xi} = \cos\bar{\theta}, \quad \hat{\eta} = -\sin\bar{\theta} \quad \text{at } L = 0. \tag{4.16}$$

These conditions together with the downstream boundary conditions (4.7), (4.9) and (4.11), and the differential equations (4.1)–(4.3) completely specify the cable response. In particular $\hat{\xi}(L)$ and $\hat{\eta}(L)$ may be determined by numerical integration.

An element at an arc length l from the ship is perturbed from its steady towing position by $(x'(l,t), 0, z'(l,t))$, where $x'(l,t) = \mathrm{Re}\,(l_A \hat{x}(L)\,e^{i\omega t})$, $z'(l,t) = \mathrm{Re}\,(l_A \hat{z}(L)\,e^{i\omega t})$, with $L = l/l_A$ and

$$\hat{x}(L) = \hat{\xi}(L)\cos\bar{\theta} - \hat{\eta}(L)\sin\bar{\theta}, \quad \hat{z}(L) = \hat{\xi}(L)\sin\bar{\theta} + \hat{\eta}(L)\cos\bar{\theta}, \tag{4.17}$$

for $0 \leqslant L \leqslant L_C$. The vibration of the cylinder is described by

$$\hat{x}(L) = \hat{\xi}(L_C), \quad \hat{z}(L) = Y(L - L_C) \quad \text{for } L_C \leqslant L \leqslant L_C + 1 - \epsilon_A/C_T, \tag{4.18}$$

where $Y(X)$ is defined in (4.8). The magnitude and phase of the complex displacements $\hat{x}(L)$ and $\hat{z}(L)$ are plotted in figure 10 for three different values of Ω and the usual cable and cylinder geometry ($a_A = 8.25 \times 10^{-5} l_A$, $gl_A/U^2 = 578$, $l_C = 3.7 l_A$, $a_C = 4.125 \times 10^{-5} l_A$, $\sigma = 2.8$, $C_T = 0.0025$, $C_N = 0.75 C_T$ and $C_D = 1.2$). Before discussing the structure displayed in these graphs it is appropriate to investigate the limits of low and high frequency where analytical expressions for the displacements can be derived.

Over most of its length the mean cable inclination is constant and equal to the critical angle $\bar{\theta}_c$, and then the equations for $\hat{\xi}(L)$ and $\hat{\eta}(L)$ simplify considerably. Let us suppose that $\theta = \bar{\theta}_c$ is a good approximation to the actual cable position for L in the range $0 \leqslant L \leqslant L_0$.

When $\bar{\theta}$ is constant, (4.1) simply states that $\hat{\xi}$ is independent of position. Hence after applying the boundary condition (4.16) we can deduce that the in-line deflections are given by

$$\hat{\xi}(L) = \cos\bar{\theta}_c \quad \text{for } 0 \leqslant L \leqslant L_0. \tag{4.19}$$

As discussed in §3, the differential equation (2.18) for the mean tension has constant coefficients in the range $0 \leqslant L \leqslant L_0$. It can be readily integrated to give (see equation (3.8)),

$$\bar{\tau}(L) = \bar{\tau}(L_0) + [(\sigma - 1)\epsilon^2\alpha \sin\bar{\theta}_c + \epsilon C_T \cos\bar{\theta}_c](L_0 - L).$$

When this and (4.19) are substituted into (4.3) it simplifies to

$$(L_1 - L)\frac{d^2\hat{\eta}}{dL^2} - f_2\frac{d\hat{\eta}}{dL} + h_2\hat{\eta} = g_2, \tag{4.20}$$

$\hat{\eta}(L)$ satisfies an inhomogeneous second-order differential equation. L_1, f_2, g_2 and h_2 are all constants:

$$L_1 = L_0 + \frac{\bar{\tau}(L_0)}{(\sigma - 1)\epsilon^2\alpha \sin\bar{\theta}_c + \epsilon C_T \cos\bar{\theta}_c}, \tag{4.21a}$$

$$f_2 = \frac{(\sigma - 1)\epsilon\alpha \sin\bar{\theta}_c + (C_N + 2C_D \sin\bar{\theta}_c/\pi)\cos\bar{\theta}_c}{(\sigma - 1)\epsilon\alpha \sin\bar{\theta}_c + C_T \cos\bar{\theta}_c}, \tag{4.21b}$$

$$g_2 = -\frac{i\Omega C_N \sin\bar{\theta}_c \cos^2\bar{\theta}_c}{(\sigma - 1)\epsilon\alpha \sin\bar{\theta}_c + C_T \cos\bar{\theta}_c}, \tag{4.21c}$$

$$h_2 = \frac{(\sigma + 1)\epsilon\Omega^2 - i\Omega(C_N(1 + \sin^2\bar{\theta}_c) + 2C_D \sin\bar{\theta}_c/\pi)}{(\sigma - 1)\epsilon\alpha \sin\bar{\theta}_c + C_T \cos\bar{\theta}_c}. \tag{4.21d}$$

When C_N is set equal to zero and the gravity term $(\sigma-1)\,\epsilon\alpha\sin\bar{\theta}_c$ is neglected, Lyon's (1962) equation for the in-plane deflection of a string is recovered from (4.20).

The particular integral of (4.20) is $\hat{\eta}(L) = g_2/h_2$. The asymptotic forms of the general solution of a similar equation were evaluated in §3. In particular, (3.11) shows the low-frequency asymptotic solution to be

$$\hat{\eta}(L) \sim R_3\left\{1-\frac{h_2}{f_2}(L_1-L)\right\}+S_3(L_1-L)^{1-f_2}\left\{1-\frac{h_2}{2-f_2}(L_1-L)\right\}+\frac{g_2}{h_2}, \tag{4.22}$$

for $0 \leqslant L \leqslant L_0$. R_3 and S_3 can be determined precisely from boundary conditions at $L = 0$ and L_0. But calculation of $\hat{\eta}(L_0)$ requires a numerical integration of equations (4.1)–(4.3) over a region near the downstream end of the cable where $\bar{\theta}$ varies rapidly. Instead we argue, as we did in §3, that since f_2 is large and positive the second term in (4.22) is very much smaller than the first once L is appreciably less than L_0. This means that $\hat{\eta}(L)$ simplifies to

$$\hat{\eta}(L) = R_3\left\{1-\frac{h_2}{f_2}(L_1-L)\right\}+\frac{g_2}{h_2}, \tag{4.23}$$

in the range $0 \leqslant L \ll L_0$. The remaining constant R_3 may then be evaluated from the upstream boundary condition (4.16) to give

$$\hat{\eta}(L) = -\sin\bar{\theta}_c\left(1+\frac{h_2}{f_2}L\right)-\frac{g_2}{f_2}L. \tag{4.24}$$

The expressions for $\hat{\xi}(L)$ and $\hat{\eta}(L)$ in (4.19) and (4.24) respectively may be combined to calculate $\hat{x}(L)$ and $\hat{z}(L)$ from (4.17);

$$\hat{x}(L) = 1+\sin\bar{\theta}_c\left(\frac{g_2+h_2\sin\bar{\theta}_c}{f_2}\right)L, \tag{4.25a}$$

$$\hat{z}(L) = -\cos\bar{\theta}_c\left(\frac{g_2+h_2\sin\bar{\theta}_c}{f_2}\right)L. \tag{4.25b}$$

This low-frequency asymptotic form is plotted in figure 10 for comparison with the exact solution. There is good agreement for $\Omega = 0.1$.

The low-frequency results have a simple physical interpretation. When the parameters f_2, g_2 and h_2 in (4.25) are rewritten explicitly, the expressions for $\hat{x}(L)$ and $\hat{z}(L)$ become

$$\hat{x}(L) = 1-\frac{2\mathrm{i}\Omega(C_N+C_D\sin\bar{\theta}_c/\pi)\,L\sin^2\bar{\theta}_c}{(\sigma-1)\,\epsilon\alpha\sin\bar{\theta}_c+(C_N+2C_D\sin\bar{\theta}_c/\pi)\cos\bar{\theta}_c}, \tag{4.26a}$$

and

$$\hat{z}(L) = \frac{2\mathrm{i}\Omega(C_N+C_D\sin\bar{\theta}_c/\pi)\,L\sin\bar{\theta}_c\cos\bar{\theta}_c}{(\sigma-1)\,\epsilon\alpha\sin\bar{\theta}_c+(C_N+2C_D\sin\bar{\theta}_c/\pi)\cos\bar{\theta}_c}, \tag{4.26b}$$

for small values of Ω. We will now demonstrate that these displacements correspond to a quasi-static oscillation in which the cable remains straight at the appropriate instantaneous critical angle. The cable follows the displacement of the towing point and its inclination alters as changes in the towing velocity change the critical angle. For such a motion the perturbation in displacement a distance l along the cable would be given by

$$x'(l,t) = x'(0,t)-\theta_c' l\sin\bar{\theta}_c, \quad z'(l,t) = \theta_c' l\cos\bar{\theta}_c, \tag{4.27}$$

where θ_c' denotes a change in the critical angle. θ_c' will now be evaluated to show that these expressions are identical to those given in (4.26).

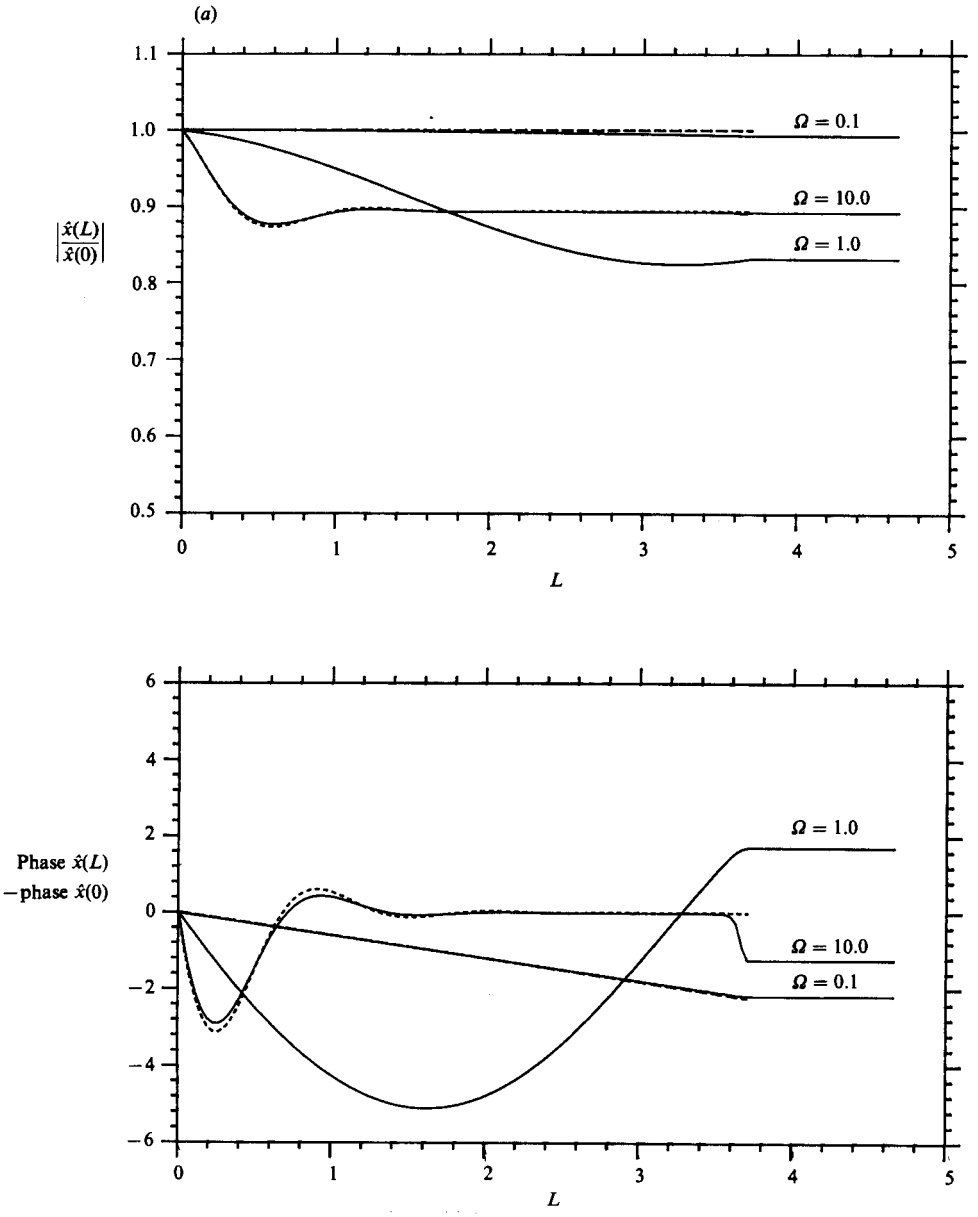

FIGURE 10(*a*). For caption see facing page.

The critical angle for a towing speed U is given in equation (2.11):

$$(\sigma-1)\cos\bar{\theta}_c\frac{a_C g}{U^2}=\left(C_N+\frac{C_D}{\pi}\sin\bar{\theta}_c\right)\sin\bar{\theta}_c.$$

The change in critical angle, due to a small change in the towing speed from U to $U+u'$, can be found by differentiating this equation

$$\theta_c'=-\frac{2(\sigma-1)\cos\bar{\theta}_c a_C g/U^2}{(\sigma-1)\sin\bar{\theta}_c a_C g/U^2+(C_N+2C_D\sin\bar{\theta}_c/\pi)\cos\bar{\theta}_c}\frac{u'}{U}. \tag{4.28}$$

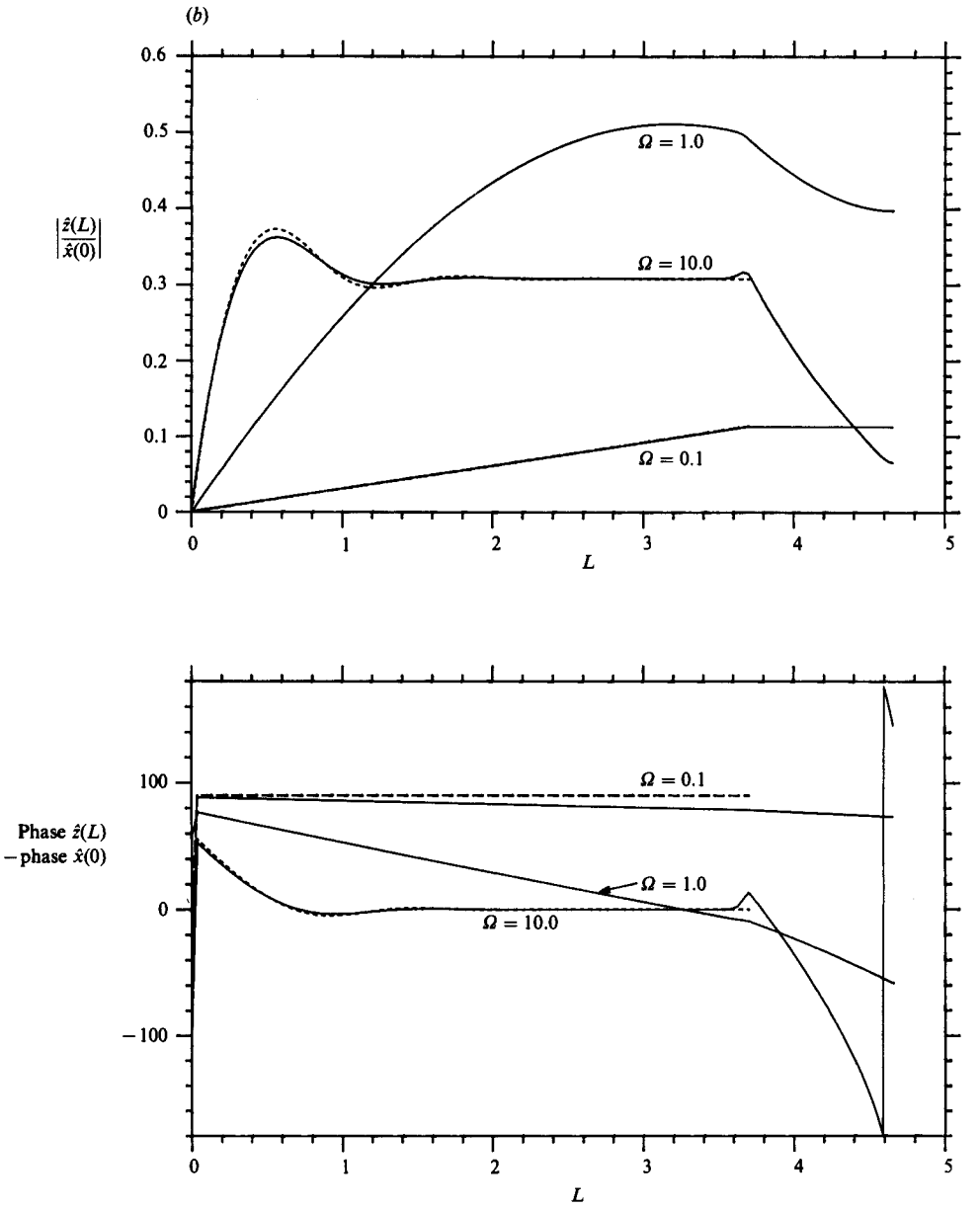

FIGURE 10. Plots of the variation in the magnitude and phase of the in-plane displacement of the cable and cylinder as a function of L, the non-dimensional arc length from the towing point for three values of Ω. $C_T = 0.0025$, $C_D = 1.2$, $C_N = 0.75C_T$, $\sigma = 2.8$, $l_C/l_A = 3.7$, $gl_A/U^2 = 578$, $a_C/l_A = 4.125 \times 10^{-5}$ and $a_A/l_A = 8.25 \times 10^{-5}$. (*a*) The horizontal, and (*b*) the vertical displacements are given by $x'(l, t) = \mathrm{Re}\,(l_A \hat{x}(L)\, e^{i\omega t})$, $z'(l, t) = \mathrm{Re}\,(l_A \hat{z}(L)\, e^{i\omega t})$, with $l = Ll_A$, $\omega = \Omega U/l_A$. The cylinder extends from $L = 3.7$ to $L = 4.7$. ---, low-frequency asymptotic form (equation (4.25)); - - - - -, high-frequency asymptotic form (equation (4.34)).

Equation (2.11) may be used to rewrite the numerator in terms of C_N and C_D, to give

$$\theta_c' = -\frac{2(C_N + C_D \sin\bar{\theta}_c/\pi)\sin\bar{\theta}_c}{(\sigma-1)\sin\bar{\theta}_c\, a_C\, g/U^2 + (C_N + 2C_D \sin\bar{\theta}_c/\pi)\cos\bar{\theta}_c}\frac{u'}{U}. \tag{4.29}$$

In the particular case considered here $x'(0, t) = \mathrm{Re}\,(l_A\, e^{i\omega t})$ and $u' = \mathrm{Re}\,(-i\omega l_A\, e^{i\omega t})$. Using (4.29) in (4.27) therefore shows that

$$\hat{x}(L) = 1 - \frac{2i\Omega(C_N + C_D \sin\bar{\theta}_c/\pi)\, L \sin^2\bar{\theta}_c}{(\sigma-1)\,\epsilon\alpha \sin\bar{\theta}_c + (C_N + 2C_D \sin\bar{\theta}_c/\pi)\cos\bar{\theta}_c}, \tag{4.30a}$$

$$\hat{z}(L) = \frac{2i\Omega(C_N + C_D \sin\bar{\theta}_c/\pi)\, L \sin\bar{\theta}_c \cos\bar{\theta}_c}{(\sigma-1)\,\epsilon\alpha \sin\bar{\theta}_c + (C_N + 2C_D \sin\bar{\theta}_c/\pi)\cos\bar{\theta}_c}. \tag{4.30b}$$

This is identical to (4.26) showing that the low-frequency solution of the differential equation does indeed describe the quasi-static displacements evaluated here.

For large Ω, the complementary function of the second-order differential equation (4.20) is given approximately by a WKB method in the way outlined in §3. By comparison with (3.19)

$$\hat{\eta}(L) \sim h_2^{-\frac{1}{4}}(L_1 - L)^{\frac{1}{4}-\frac{1}{2}f_2}\{R_4 \exp[2ih_2^{\frac{1}{2}}(L_1-L)^{\frac{1}{2}}] + S_4 \exp[-2ih_2^{\frac{1}{2}}(L_1-L)^{\frac{1}{2}}]\} + \frac{g_2}{h_2}, \tag{4.31}$$

for $0 \leqslant L \leqslant L_0$. The root of $h_2^{\frac{1}{2}}$ is to be chosen so that it has negative imaginary part.

Rather than apply boundary conditions at L_0 to evaluate R_4 and S_4 exactly, we again note that for L appreciably less than L_0 the second term in (4.31) is much smaller than the first. Hence

$$\hat{\eta}(L) \sim R_4\, h_2^{-\frac{1}{4}}(L_1 - L)^{\frac{1}{4}-\frac{1}{2}f_2} \exp[2ih_2^{\frac{1}{2}}(L_1-L)^{\frac{1}{2}}] + \frac{g_2}{h_2}, \tag{4.32}$$

for $0 \leqslant L \ll L_0$. R_4 may be found from the upstream boundary condition (4.16) to give

$$\hat{\eta}(L) = \frac{g_2}{h_2} - \left(\frac{g_2}{h_2} + \sin\bar{\theta}_c\right)(1 - L/L_1)^{\frac{1}{4}-\frac{1}{2}f_2} \exp[-2ih_2^{\frac{1}{2}}\{L_1^{\frac{1}{2}} - (L_1-L)^{\frac{1}{2}}\}]. \tag{4.33}$$

The expressions for $\hat{\xi}(L)$ and $\hat{\eta}(L)$ in (4.19) and (4.33) respectively may be combined to calculate $\hat{x}(L)$ and $\hat{z}(L)$ from (4.17)

$$\hat{x}(L) = \cos^2\bar{\theta}_c - \frac{g_2}{h_2}\sin\bar{\theta}_c + \left(\frac{g_2}{h_2} + \sin\bar{\theta}_c\right)\sin\bar{\theta}_c(1 - L/L_1)^{\frac{1}{4}-\frac{1}{2}f_2} \times \exp[-2ih_2^{\frac{1}{2}}\{L_1^{\frac{1}{2}} - (L_1-L)^{\frac{1}{2}}\}], \tag{4.34a}$$

$$\hat{z}(L) = \sin\bar{\theta}_c\cos\bar{\theta}_c + \frac{g_2}{h_2}\cos\bar{\theta}_c - \left(\frac{g_2}{h_2} + \sin\bar{\theta}_c\right)\cos\bar{\theta}_c(1 - L/L_1)^{\frac{1}{4}-\frac{1}{2}f_2} \times \exp[-2ih_2^{\frac{1}{2}}\{L_1^{\frac{1}{2}} - (L_1-L)^{\frac{1}{2}}\}]. \tag{4.34b}$$

These expressions are plotted in figure 10 for comparison with the exact solution and the agreement is good.

Figure 10 shows the transmission of in-plane oscillations along the cable to be quite different from the transmission of transverse oscillations investigated in §3. The cable acts as a low-pass filter for transverse deflections, high-frequency oscillations being effectively attenuated as they propagate down the cable. Hence little horizontal

array motion would be expected at moderate and high frequencies. The situation is quite different for vertical fluctuations since figure 10 shows there to be appreciable transmission along the cable for all frequencies.

The asymptotic form (4.34) can be used to calculate transmission of in-plane vibrations at high frequencies. The exponential terms in (4.34) decay rapidly away from $L = 0$, leaving only the constant terms. For typical cable parameters $\sin\bar{\theta}_c$ is much bigger than g_2/h_2 and so for $L \gg 0$

$$\hat{x}(L) \sim \cos^2\bar{\theta}_c, \quad \hat{z}(L) \sim \sin\bar{\theta}_c \cos\bar{\theta}_c. \tag{4.35}$$

The derivation of the high-frequency asymptotic form demonstrates how these constant terms arise. Horizontal unit forcing of the upstream end produces a longitudinal cable displacement $\hat{\xi}(0) = \cos\bar{\theta}_c$ and a normal displacement $\hat{\eta}(0) = -\sin\bar{\theta}_c$ (see equation (4.16)). Since the cable is straight the tugging produced by the in-line displacement is the same all along the cable, as shown by (4.19). While equation (4.33) shows that at high frequencies the normal displacement is significantly attenuated as disturbances travel down the cable. Hence, at an appreciable distance along the cable, the remaining displacement is $\cos\bar{\theta}_c$ at an angle $\bar{\theta}_c$ to the horizontal. Resolving this vertically and horizontally leads to displacements of the form shown in (4.35).

The detailed form of the vibration of the cable is of limited interest. What is relevant is how much vibration is transmitted from the towing ship to the sonar array along the cable. This is described by the two ratios $\hat{x}(L_C)/\hat{x}(0)$ and $\hat{z}(L_C)/\hat{x}(0)$. These transfer functions are plotted in figure 11 as a function of a non-dimensional frequency $\tilde{\Omega}$, defined by

$$\tilde{\Omega} = \Omega L_C. \tag{4.36}$$

In terms of the dimensional frequency ω

$$\tilde{\Omega} = \omega l_C/U. \tag{4.37}$$

$\hat{x}(L_C)$ gives an in-line perturbation to the leading edge of the cylinder. This results in a uniform in-line displacement of the whole array as described by (4.18). The transverse displacement of the leading edge of the cylinder, $\hat{z}(L_C)$, produces waves that propagate along the cylinder in the way determined in Part 1.

The low- and high-frequency asymptotic forms for the cable displacement were derived for positions away from the cable end. But figure 10 shows that they even give a reasonable approximation to the displacement at the downstream end of the cable, and we will use them here to interpret the numerical results for the transfer function. Equations (4.30) and (4.35) imply that

$$\frac{\hat{z}(L_C)}{\hat{x}(0)} = \frac{2i\tilde{\Omega}\sin\bar{\theta}_c\cos\bar{\theta}_c(C_N + C_D\sin\bar{\theta}_c/\pi)}{(\sigma-1)\,\epsilon\alpha\sin\bar{\theta}_c + (C_N + 2C_D\sin\bar{\theta}_c/\pi)\cos\bar{\theta}_c} \quad \text{for } \Omega \ll 1, \tag{4.38}$$

and

$$\frac{\hat{z}(L_C)}{\hat{x}(0)} = \sin\bar{\theta}_c\cos\bar{\theta}_c, \quad \frac{\hat{x}(L_C)}{\hat{x}(0)} = \cos^2\bar{\theta}_c \quad \text{for } \Omega \gg 1. \tag{4.39}$$

Figure 11 shows that the numerical solution for $|\hat{z}(L_C)|$ increases linearly with $\tilde{\Omega}$, for small values of $\tilde{\Omega}$. This is in agreement with the low-frequency asymptotic form (4.38). At high frequencies the two transfer functions $\hat{x}(L_C)/\hat{x}(0)$ and $\hat{z}(L_C)/\hat{x}(0)$ are found to be practically independent of frequency, as predicted by the high-frequency asymptotic form in (4.39).

The transfer function for the vertical displacement, as shown in figure 11, has a

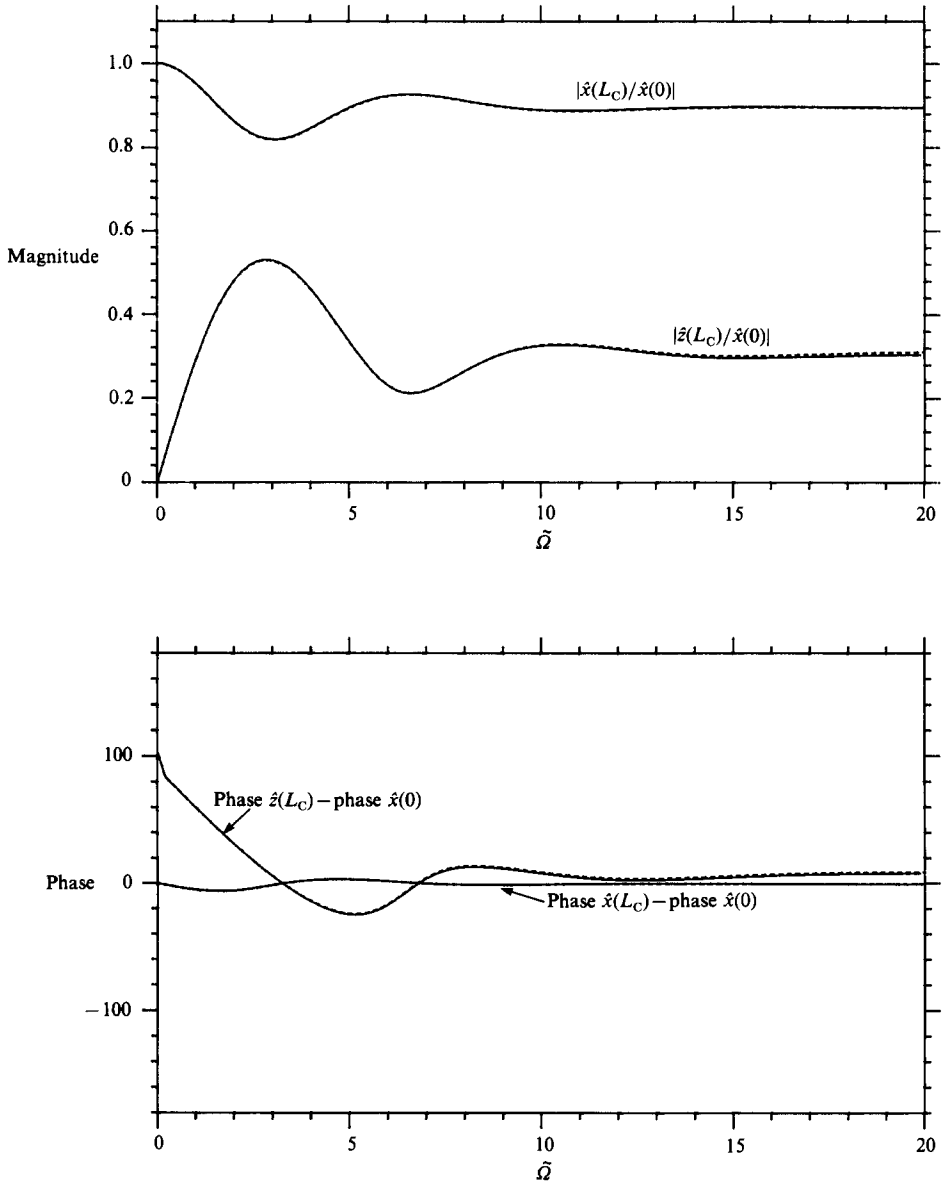

FIGURE 11. The variation of the transfer functions $\hat{x}(L_C)/\hat{x}(0)$ and $\hat{z}(L_C)/\hat{x}(0)$, describing transmission across the cable, with non-dimensional frequency $\tilde{\Omega}$. The value of C_N is shown to have negligible effect on the cable motion. The other cable and cylinder parameters are as in figure 10. - - - - -, $C_N = 0.25C_T$; ——, $C_N = 0.75C_T$.

maximum at a non-dimensional frequency of about 2.8. Returning to dimensional parameters, this means that perturbations in the ship's position are most effectively transformed into vertical oscillations of the array at a frequency $\omega \sim 2.8U/l_C$. Towed arrays have been observed to execute oscillations of considerable amplitudes with frequencies of this order.

The transfer functions $\hat{x}(L_C)/\hat{x}(0)$ and $\hat{z}(L_C)/\hat{x}(0)$ are plotted in figure 11 for two different values of the normal drag coefficient C_N. The two curves overlie showing that the value of C_N has little influence on the cable motion.

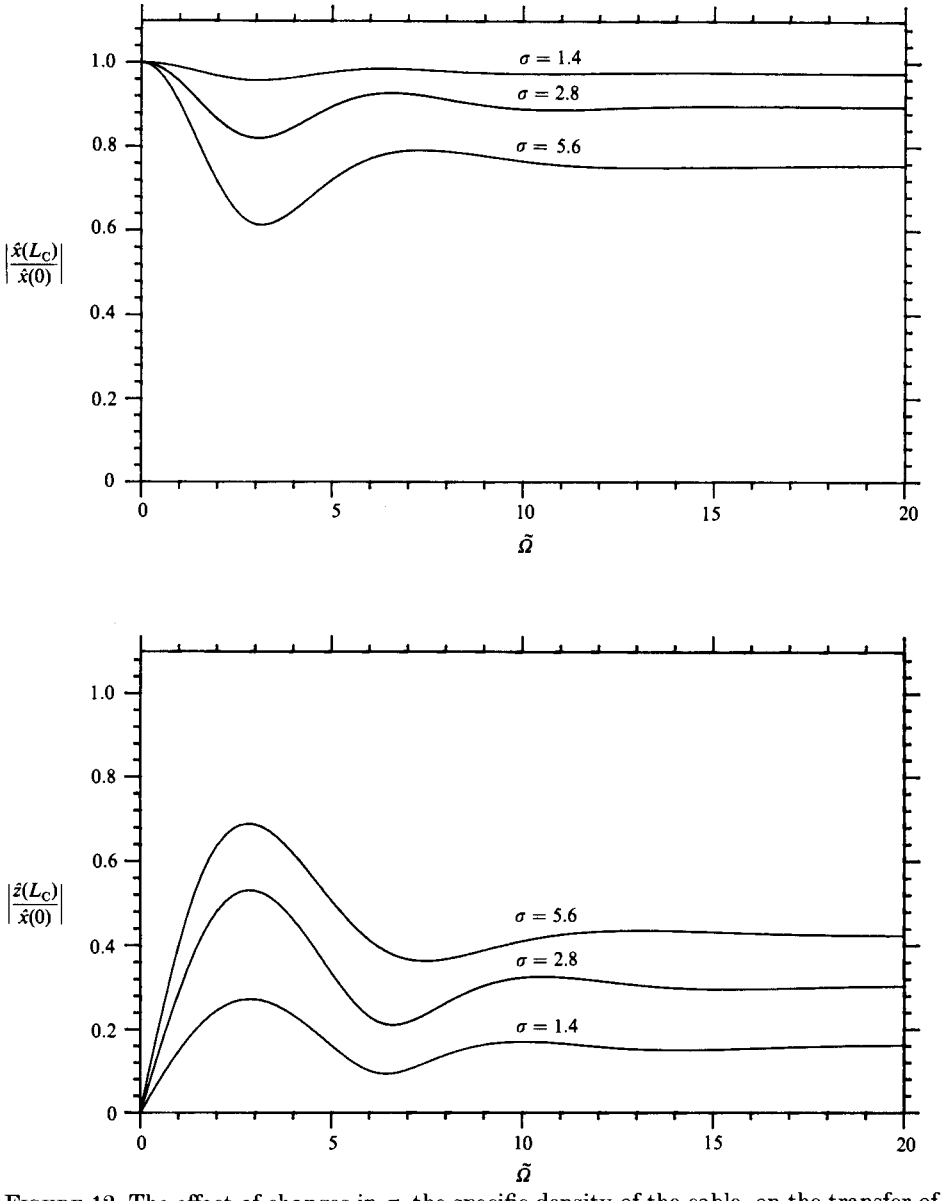

FIGURE 12. The effect of changes in σ, the specific density of the cable, on the transfer of in-plane oscillations along the cable. $l_C/l_A = 3.7$, $gl_A/U^2 = 578$, $a_C/l_A = 4.125 \times 10^{-5}$ and $a_A/l_A = 8.25 \times 10^{-5}$, $C_T = 0.0025$, $C_N = 0.75C_T$ with $C_D = 1.2$.

Figures 12–15 demonstrate the effect of varying the cable parameters for a given cylinder and fixed drag coefficients. In these diagrams $a_A = 8.25 \times 10^{-5} l_A$, $C_T = 0.0025$, $C_N = 0.75C_T$, $C_D = 1.2$ and the cable properties are varied. It is interesting to note that the non-dimensional frequency, at which the transfer function for the vertical displacements is maximal, is the same in all the diagrams. It is uninfluenced by these differences in the cable parameters.

Figure 12 shows the effect of changes in σ, the specific gravity of the cable. The magnitude of the vertical vibration transmitted along the cable at a particular

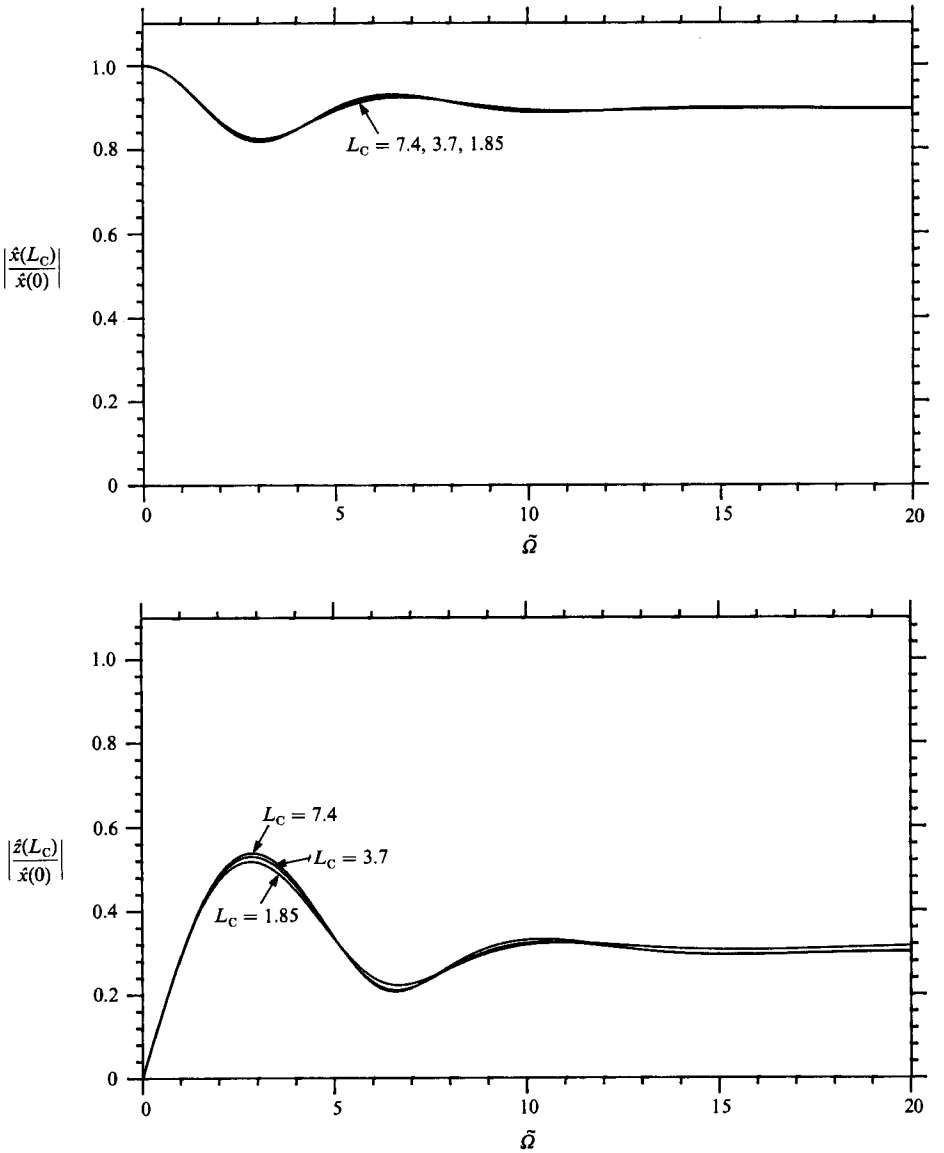

FIGURE 13. The effect of changes in $L_C = l_C/l_A$, the non-dimensional length of the cable, on the transfer of in-plane oscillations along the cable $\sigma = 2.8$, $gl_A/U^2 = 578$, $a_C/l_A = 4.125 \times 10^{-5}$. The cylinder geometry and drag coefficients are as in figure 12.

frequency is found to increase as the density of the cable is increased. This could have been anticipated from the high-frequency asymptotic form (4.39) which gives $\hat{z}(L_C) = \hat{x}(0) \sin\bar{\theta}_c \cos\bar{\theta}_c$ for large values of Ω. An increase in the cable density, for fixed values of the other parameters, has the effect of increasing the critical angle $\bar{\theta}_c$. It therefore follows that a denser cable leads to more vertical displacements of the array at high frequencies.

Figure 13 shows that changes in the cable length have virtually no effect on the transmission across the cable at a fixed non-dimensional frequency. This is consistent with our low- and high-frequency asymptotic forms in which $\hat{x}(L_C)/\hat{x}(0)$ and

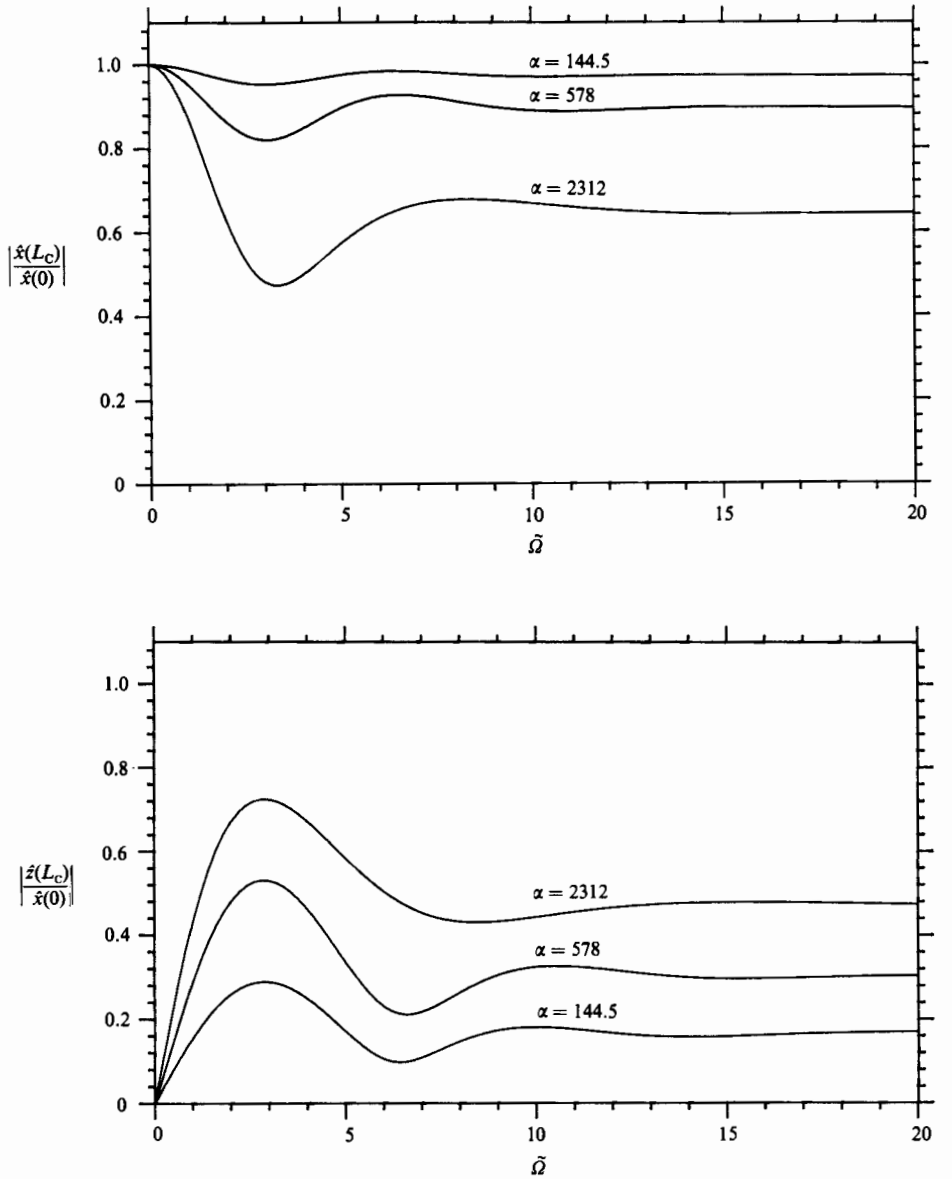

FIGURE 14. The effect of changes in $\alpha = gl_A/U^2$, the inverse-square Froude number, on the transfer of in-plane oscillations along the cable, $\sigma = 2.8$, $l_C/l_A = 3.7$, $a_C/l_A = 4.125 \times 10^{-5}$. The cylinder geometry and drag coefficients are as in figure 12.

$\hat{z}(L_C)/\hat{x}(0)$ are independent of L_C for a fixed value of $\tilde{\Omega}$. It should be remembered that $\Omega = \omega l_C/U$. Hence, when investigating the propagation of disturbances of a particular dimensional frequency ω, changes in l_C change the appropriate value of $\tilde{\Omega}$. How this affects the amplitude of the transmitted vibration will depend on the actual values of $\tilde{\Omega}$.

The effect of altering the Froude number is shown in figure 14. When the towing velocity U is increased, the amplitude of the vertical vibration transmitted along the cable at fixed $\tilde{\Omega}$ decreases. Again this can be explained by reference to the low- and

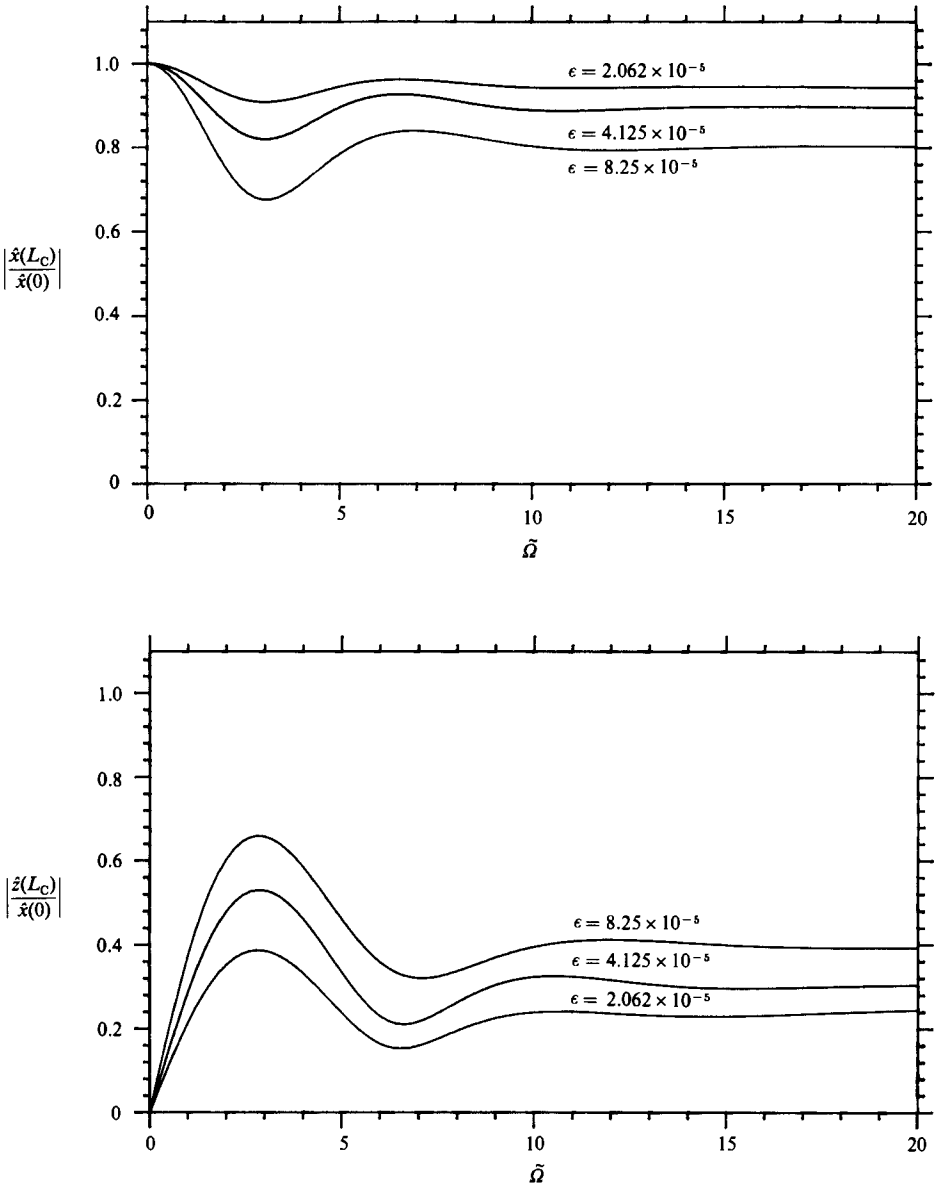

FIGURE 15. The effect of changes in cable radius, $\epsilon = a_C/l_A$, on the transfer of in-plane oscillations along the cable. $\sigma = 2.8$, $l_C/l_A = 3.7$, $gl_A/U^2 = 578$. The cylinder geometry and drag coefficients are as in figure 12.

high-frequency asymptotic forms, and by noting that an increase in velocity tends to reduce the critical angle. For a fixed frequency ω, a change in U will also shift the non-dimensional frequency $\tilde{\Omega} = \omega l_C/U$.

Finally figure 15 demonstrates the influence of the value of the cable diameter on the transfer function. Once again the same trends are observed. An increase in the cable diameter leads to a larger critical angle, and hence to an increase in the amplitude of the vertical vibration transmitted through the cable to the sonar array.

5. Conclusions

An analytical expression was obtained in Part 1 relating the linear transverse deflection of any part of a neutrally buoyant cylinder to the deflection of its leading edge. This paper completes the description of cylinder motion by determining how the effects of perturbations in the position of the towing vessel propagate down the cable to excite the cylinder and hence perturb the sonar array.

Since the cylinder is neutrally buoyant, its mean geometry under steady towing is simple: it is straight and horizontal. The cable, however, being heavier than water, is inclined to the direction of motion. In practice the tension in the cable is sufficiently large to ensure that over most of its length the mean cable geometry is a straight line, inclined at the critical angle to the horizontal. This is the angle of cable inclination for which the mean normal drag and gravity forces on the cable balance. In considering linear perturbations of the cable from this steady-state position, the cylinder deflection determined in Part 1 acts as a downstream boundary condition for the cable motion.

The stability of the cable and cylinder under constant towing conditions may be investigated by seeing whether free modes in which there is no perturbation in the position of the upstream end of the cable grow or decay in time. Numerical calculations showed the system to be stable for typical geometries. Since the cable and cylinder are stable, it is appropriate to investigate their response to forcing at the towing point. Transverse oscillations, in a horizontal direction perpendicular to the mean towing velocity, entirely decouple from in-plane vibrations.

Meandering of the ship produces transverse oscillations of the cable and cylinder. For low frequencies these disturbances propagate down the cable with little change in amplitude, while higher-frequency disturbances are significantly attenuated. The details of the cable vibration are of limited interest. The primary interest is in how much vibration is transmitted from the ship to the cylinder and hence to the sonar array. This transfer function was found to depend strongly on the non-dimensional frequency $\omega l_c/U$ and only weakly on the other cable parameters. The theory compares well with the experimental data of Kennedy & Strahan (1981).

Perturbations in the ship's speed generate oscillations of the cable and cylinder in a vertical plane. The propagation of these disturbances from the ship to the cylinder along the cable is effective at all frequencies. At low frequencies the cable's motion is quasi-static: the cable follows the displacement of the towing point with its inclination changing as changes in the towing speed alter the critical angle. At high frequencies any unsteady motion normal to the cable rapidly decays as the distance along the cable increases, while any in-line oscillation is unchanged. This leads to the vertical displacement at the leading edge of the array being a factor $\sin\bar{\theta}_c \cos\bar{\theta}_c$ smaller than the perturbation in the ship's position at high frequencies. A numerical solution is required to determine the transfer of vibrations along the cable at a general frequency. This shows that perturbations in the ship's position are most effectively transformed into vertical oscillations of the array at a frequency of $2.8U/l_c$. The effect of the cable properties on transmission along the cable has been investigated. The transfer function depends on the value of the non-dimensional frequency $\omega l_c/U$. Parameter changes, which increase the cable critical angle, increase the proportion of the forcing from the towing point transformed into vertical array motion at a fixed value of $\omega l_c/U$.

We have developed a simple means of determining the sonar array shape from linear changes in the ship's towing velocity. In particular it has been possible to see

how the cable parameters and the frequency of oscillation affect the amplitude of the sonar array motion. This leads to an indication of how the cable geometry should be chosen to minimize array oscillation.

This work has been carried out with the support of Topexpress Ltd and the Procurement Executive, Ministry of Defence.

Appendix. Derivation of the equations of cable motion

The position vector of the cable element l at time t has been decomposed into steady-state and fluctuating components in equations (2.12) and (2.13)

$$\boldsymbol{r}(l, t) = \bar{\boldsymbol{r}}(l, t) + \boldsymbol{r}'(l, t), \tag{A 1}$$

with

$$\boldsymbol{r}'(l, t) = (\xi \cos\bar{\theta} - \eta \sin\bar{\theta}, \zeta, \xi \sin\bar{\theta} + \eta \cos\bar{\theta}). \tag{A 2}$$

The instantaneous tangential direction $\boldsymbol{s}$ can be determined from the derivative $\partial \boldsymbol{r}/\partial l$ to give

$$\boldsymbol{s} = (\cos\bar{\theta}, 0, \sin\bar{\theta}) + \left(\frac{\partial\xi}{\partial l}\cos\bar{\theta} - \frac{\partial\eta}{\partial l}\sin\bar{\theta}, \frac{\partial\zeta}{\partial l}, \frac{\partial\xi}{\partial l}\sin\bar{\theta} + \frac{\partial\eta}{\partial l}\cos\bar{\theta}\right) + (-\xi\sin\bar{\theta} - \eta\cos\bar{\theta}, 0, \xi\cos\bar{\theta} - \eta\sin\bar{\theta})\frac{\mathrm{d}\bar{\theta}}{\mathrm{d}l}, \tag{A 3}$$

ξ, ζ, η are all small quantities and their products may be neglected. The use of the condition that $\boldsymbol{s}$ is a unit vector in (A 3) shows that

$$\frac{\partial\xi}{\partial l} = \eta\frac{\mathrm{d}\bar{\theta}}{\mathrm{d}l}. \tag{A 4}$$

This is used in (2.14). With this relationship between $\partial\xi/\partial l$ and η, $\boldsymbol{s}$ simplifies to

$$\boldsymbol{s} = (\cos\bar{\theta}, 0, \sin\bar{\theta}) + (-\sin\bar{\theta}, 0, \cos\bar{\theta})\,\theta' + (0, \partial\zeta/\partial l, 0). \tag{A 5}$$

The angle θ' has been introduced, where

$$\theta' = \xi\frac{\mathrm{d}\bar{\theta}}{\mathrm{d}l} + \frac{\partial\eta}{\partial l}. \tag{A 6}$$

Equation (A 5) demonstrates that θ' is the linear perturbation in the angle the cable makes with the positive x-axis.

The velocity of the cable element may be found simply just by differentiating the position vector. With $\boldsymbol{r}'$ expressed as in (A 2), this gives

$$\boldsymbol{v} = (-U, 0, 0) + (\dot{\xi}\cos\bar{\theta} - \dot{\eta}\sin\bar{\theta}, \dot{\zeta}, \dot{\xi}\sin\bar{\theta} + \dot{\eta}\cos\bar{\theta}). \tag{A 7}$$

Differentiating again leads to

$$\boldsymbol{A} = (\ddot{\xi}\cos\bar{\theta} - \ddot{\eta}\sin\bar{\theta}, \ddot{\zeta}, \ddot{\xi}\sin\bar{\theta} + \ddot{\eta}\cos\bar{\theta}). \tag{A 8}$$

The tangential components of the cable velocity and acceleration, v_s and A_s, may be calculated by forming the scalar product of $\boldsymbol{v}$ and $\boldsymbol{A}$ with the vector $\boldsymbol{s}$ given in (A 5). When these are substituted into the tangential momentum equation (2.4a), they lead to

$$\rho_0\sigma\pi a_C^2\ddot{\xi} = \rho_0(\sigma - 1)\pi a_C^2 g(\sin\bar{\theta} + \cos\bar{\theta}\theta') + \partial T/\partial l - \rho_0(U - \dot{\xi}\cos\bar{\theta} + \dot{\eta}\sin\bar{\theta})\pi a_C C_T(-U\cos\bar{\theta} + U\sin\bar{\theta}\theta' + \dot{\xi}). \tag{A 9}$$

After the mean equation (2.7) has been subtracted from this and the resulting equation linearized in the perturbations it reduces to

$$\rho_0 \sigma \pi a_C^2 \ddot{\xi} = \rho_0(\sigma-1)\pi a_C^2 g \cos\bar{\theta}\theta' + \partial T'/\partial l$$
$$-\rho_0 U \pi a_C C_T(U \sin\bar{\theta}\theta' + (1+\cos^2\bar{\theta})\dot{\xi} - \sin\bar{\theta}\cos\bar{\theta}\dot{\eta}). \quad \text{(A 10)}$$

This equation relates the in-plane displacements to changes in tension.

The normal momentum balance described by (2.4*b*) can be treated in a similar way. It is convenient to introduce two mutually perpendicular unit vectors $\boldsymbol{n}_1$ and $\boldsymbol{n}_2$ defined by

$$\boldsymbol{n}_1 = \left(-\cos\bar{\theta}\frac{\partial\zeta}{\partial l}, 1, -\sin\bar{\theta}\frac{\partial\zeta}{\partial l}\right), \quad \text{(A 11}a\text{)}$$

$$\boldsymbol{n}_2 = (-\sin\bar{\theta} - \cos\bar{\theta}\theta', 0, \cos\bar{\theta} - \sin\bar{\theta}\theta'). \quad \text{(A 11}b\text{)}$$

The scalar products of both these vectors with $\boldsymbol{s}$ (given in equation (A 5)) is zero, showing that both $\boldsymbol{n}_1$ and $\boldsymbol{n}_2$ are normal to the instantaneous position of the cable.

The derivative $\partial\boldsymbol{s}/\partial l$ appears in (2.4*b*), and may be evaluated by differentiating (A 5) term by term;

$$\frac{\partial \boldsymbol{s}}{\partial l} = (-\sin\bar{\theta}, 0, \cos\bar{\theta})\frac{\mathrm{d}}{\mathrm{d}l}(\bar{\theta}+\theta') - (\cos\bar{\theta}, 0, \sin\bar{\theta})\frac{\mathrm{d}\bar{\theta}}{\mathrm{d}l}\theta' + \left(0, \frac{\partial^2\zeta}{\partial l^2}, 0\right). \quad \text{(A 12)}$$

The components of $\partial\boldsymbol{s}/\partial l$, $\boldsymbol{g}$, $\boldsymbol{v}$ and $\boldsymbol{A}$ in the directions of the two vectors $\boldsymbol{n}_1$ and $\boldsymbol{n}_2$ may be determined from the corresponding scalar product. This shows that the $\boldsymbol{n}_1$ component of momentum balance is

$$\rho_0(\sigma+1)\pi a_C^2 \ddot{\zeta} = -\rho_0(\sigma-1)\pi a_C^2 g \sin\bar{\theta}\frac{\partial\zeta}{\partial l} + \bar{T}\frac{\partial^2\zeta}{\partial l^2}$$
$$-\rho_0 a_C U(C_D \sin\bar{\theta} + \pi C_N)\left(\dot{\zeta} + U\cos\bar{\theta}\frac{\partial\zeta}{\partial l}\right). \quad \text{(A 13)}$$

The remaining equation of motion is the $\boldsymbol{n}_2$-component of momentum balance equation (2.4*b*);

$$\rho_0(\sigma+1)\pi a_C^2 \ddot{\eta} = \rho_0(\sigma-1)\pi a_C^2 g(\cos\bar{\theta} - \sin\bar{\theta}\theta') + T\frac{\partial}{\partial l}(\bar{\theta}+\theta')$$
$$-\rho_0 a_C\{C_D(U\sin\bar{\theta} + U\cos\bar{\theta}\theta' + \dot{\eta}) + \pi C_N(U + \sin\bar{\theta}\dot{\eta}$$
$$-\cos\bar{\theta}\dot{\xi})\}(U\sin\bar{\theta} + U\cos\bar{\theta}\theta' + \dot{\eta}). \quad \text{(A 14)}$$

Once the mean normal momentum equation (2.8) is subtracted from (A 14) the resulting equation reduces to

$$\rho_0(\sigma+1)\pi a_C^2 \ddot{\eta} = -\rho_0(\sigma-1)\pi a_C^2 g \sin\bar{\theta}\theta' + T'\frac{\mathrm{d}\bar{\theta}}{\mathrm{d}l} + \bar{T}\frac{\partial\theta'}{\partial l}$$
$$-2\rho_0 a_C U C_D \sin\bar{\theta}(\dot{\eta} + U\cos\bar{\theta}\theta')$$
$$-\rho_0 a_C U \pi C_N((1+\sin^2\bar{\theta})\dot{\eta} - \sin\bar{\theta}\cos\bar{\theta}\dot{\xi} + U\cos\bar{\theta}\theta'), \quad \text{(A 15)}$$

after linearization in the perturbation quantities.

θ' is defined in (A 6) to be equal to $\partial\eta/\partial l + \xi\, \mathrm{d}\bar{\theta}/\mathrm{d}l$. The derivative, $\bar{T}\,\partial\theta'/\partial l$, therefore expands as

$$\bar{T}\frac{\partial\theta'}{\partial l} = \bar{T}\left(\frac{\partial^2\eta}{\partial l^2} + \frac{\partial\xi}{\partial l}\frac{\mathrm{d}\bar{\theta}}{\mathrm{d}l} + \xi\frac{\mathrm{d}^2\bar{\theta}}{\mathrm{d}l^2}\right). \tag{A 16}$$

Equation (A 4) states that $\partial\xi/\partial l = \eta\, \mathrm{d}\bar{\theta}/\mathrm{d}l$. The derivative $\bar{T}\,\mathrm{d}^2\bar{\theta}/\mathrm{d}l^2$ may be evaluated from the mean equations (2.7) and (2.8) to show that

$$\bar{T}\frac{\mathrm{d}^2\bar{\theta}}{\mathrm{d}l^2} = [2\rho_0(\sigma-1)\,\pi a_{\mathrm{C}}^2 g\sin\bar{\theta} + \rho_0\,\pi a_{\mathrm{C}}\,U^2 C_{\mathrm{T}}\cos\bar{\theta} + \rho_0\,a_{\mathrm{C}}\,U^2(2C_{\mathrm{D}}\sin\bar{\theta} + \pi C_{\mathrm{N}})\cos\bar{\theta}]\frac{\mathrm{d}\bar{\theta}}{\mathrm{d}l}. \tag{A 17}$$

With this expansion of $\bar{T}\,\partial\theta'/\partial l$ and θ' rewritten explicitly as $\xi\,\mathrm{d}\bar{\theta}/\mathrm{d}l + \partial\eta/\partial l$, equation (A 15) finally becomes

$$\begin{aligned}\rho_0(\sigma+1)\,\pi a_{\mathrm{C}}^2\,\ddot{\eta} = {} & -\rho_0(\sigma-1)\,\pi a_{\mathrm{C}}^2 g\sin\bar{\theta}\left(\frac{\partial\eta}{\partial l} - \xi\frac{\mathrm{d}\bar{\theta}}{\mathrm{d}l}\right) + T'\frac{\mathrm{d}\bar{\theta}}{\mathrm{d}l} + \bar{T}\left(\frac{\partial^2\eta}{\partial l^2} + \eta\left(\frac{\mathrm{d}\bar{\theta}}{\mathrm{d}l}\right)^2\right) \\ & + \rho_0\,\pi a_{\mathrm{C}}\,U^2 C_{\mathrm{T}}\cos\bar{\theta}\frac{\mathrm{d}\bar{\theta}}{\mathrm{d}l}\,\xi - 2\rho_0\,a_{\mathrm{C}}\,UC_{\mathrm{D}}\sin\bar{\theta}\left(\dot{\eta} + U\cos\bar{\theta}\frac{\partial\eta}{\partial l}\right) \\ & - \rho_0\,\pi a_{\mathrm{C}}\,UC_{\mathrm{N}}\left\{(1+\sin^2\bar{\theta})\,\dot{\eta} - \sin\bar{\theta}\cos\bar{\theta}\,\dot{\xi} + U\cos\bar{\theta}\frac{\partial\eta}{\partial l}\right\}. \end{aligned} \tag{A 18}$$

The transverse displacement ζ is a solution of (A 13) and decouples from the in-plane displacements. ξ and η are related to changes in tension and are determined by equations (A 4), (A 9) and (A 18).

REFERENCES

Cannon, T. C. & Genin, J. 1972*a* Dynamical behaviour of a materially damped flexible towed cable. *Aero. Q.* **23**, 109–120.

Cannon, T. C. & Genin, J. 1972*b* Three-dimensional dynamical behaviour of a flexible towed cable. *Aero. Q.* **23**, 201–210.

Dowling, A. P. 1988 The dynamics of towed flexible cylinders. Part 1. Neutrally buoyant elements. *J. Fluid Mech.* **187**, 507–532.

Huffman, R. R. & Genin, J. 1971 The dynamical behaviour of a flexible cylinder in a uniform flow field. *Aero. Q.* **22**, 183–195.

Kennedy, R. M. & Strahan, E. S. 1981 A linear theory of transverse cable dynamics at low frequencies. *NUSC Tech. Rep.* 6463, Naval Underwater Systems Center, Newport, Rhode Island/New London, Connecticut.

Ketchman, J. 1981 Vibration induced in towed linear underwater array cables. *IEEE J. Oceanic Engng*, OE-6, 77–87.

Lyon, R. H. 1962 The transmission of vibration by towed cables. *Bolt, Beranek and Newman Rep.* 934.

Païdoussis, M. P. 1966 Dynamics of flexible slender cylinders in axial flow: Part 1. Theory. *J. Fluid Mech.* **26**, 717–736.

Païdoussis, M. P. 1968 Stability of towed, totally submerged flexible cylinders. *J. Fluid Mech.* **34**, 273–297.

Païdoussis, M. P. 1973 Dynamics of cylindrical structures subjected to axial flow. *J. Sound Vib.* **29**, 365–385.

Phillips, W. H. 1949 Theoretical analysis of oscillations of a towed cable. *NACA Tech. Note* 1796.

SCHRAM, J. W. & REYLE, S. P. 1968 A three-dimensional dynamic analysis of a towed system. *J. Hydron.* **2**, 213–220.

TAYLOR, G. I. 1952 Analysis of the swimming of long and narrow animals. *Proc. R. Soc. Lond.* A **214**, 158–183.

ZAJAC, E. E. 1957 Dynamics and kinematics of the laying and recovery of submarine cable. *Bell Syst. Tech. J.* 1129–1207.